Ceramics International 50 (2024) 52819–52837

Contents lists available at ScienceDirect

Ceramics International

journal homepage: www.elsevier.com/locate/ceramint

Enrichment of strontium and magnesium improves the physical, mechanical and biological properties of bioactive glasses undergoing thermal treatments: New cues for biomedical applications

Devis Bellucci [a], Alessia Mazzilli [b], Andrea Martelli [a], Francesco Gerardo Mecca [a], Susanna Bonacorsi [b], Francesco Demetrio Lofaro [b], Federica Boraldi [b], Daniela Quaglino [b,1], Valeria Cannillo [a,1,*]

[a] Department of Engineering "Enzo Ferrari", Via P. Vivarelli 10, 41125, Modena, Italy
[b] Department of Life Sciences, University of Modena and Reggio Emilia, Modena, Italy

ARTICLE INFO

Handling Editor: Dr P. Vincenzini

Keywords:
bioactive glass
Strontium
Magnesium
Therapeutic ions
Mechanical properties
Thermal properties
Bioactivity
Biological performance

ABSTRACT

Bioactive glasses (BGs) have emerged as invaluable resources for bone tissue engineering due to their remarkable properties such as bioactivity, resorbability, cell compatibility, and osteoconductivity. However, these materials exhibit certain limitations when subjected to high temperatures, for their tendency to crystallize, thus leading to diminished bioactivity, reduced mechanical strength, and altered dissolution kinetics. One promising approach to counteract this problem is to reduce the alkaline element content in BGs while simultaneously adding strontium and magnesium. Building on previous studies of Bio_MS, a recently developed experimental formulation, we investigated the contributions of strontium and magnesium to the thermal, mechanical, and biological properties of various bioactive glasses, including commercially available options. Differential thermal analysis, heating microscopy, X-ray diffractometry, environmental scanning electron microscopy, measurement of the Young's modulus, simulated body fluid testing, cytotoxicity tests, cell viability, growth, adhesion and morphology were assessed through an integrated approach and compared for a complete evaluation of BGs, and of doped BGs, also undergoing thermal treatments. The results demonstrated improved thermal, mechanical and biological behaviors of the magnesium-strontium-doped BGs, thus paving the way for the development of BGs with enhanced biomedical perspectives.

1. Introduction

45S5 Bioglass® (composition: 46.1 mol% SiO_2, 26.9 mol% CaO, 24.4 mol% Na_2O, 2.6 mol% P_2O_5) stands as the pioneering bioactive glass (BG) developed in the 1970s due to the visionary work and serendipity of L.L. Hench [1]. Presently, it finds extensive use in orthopaedic and dental applications. However, 45S5 is not the only contender in the market. Indeed, extensive bioactive glass research in Finland resulted in the commercialization of the S53P4 formulation (53.8 mol.% SiO_2, 21.8 mol.% CaO, 22.7 mol.% Na_2O, 1.7 mol.% P_2O_5), known as Bonalive®. The significance of BGs lies in their remarkable propensity to elicit a positive response within the body, particularly in fostering bonding and/or interactions with host tissues [2]. This groundbreaking discovery led to the development of various BG types: conventional silicates, exemplified by 45S5, alongside phosphate-based and borate-based glasses. Essential characteristics for BG suitability in the human body encompass biocompatibility, non-cytotoxicity, immunogenicity, and bioactivity, ensuring they do not induce fibrous tissue formation or implant rejection at the application site.

A notable limitation of 45S5 and S53P4 is their challenge in being formed into amorphous bioactive glass scaffolds and, more broadly, in being sintered without experiencing significant crystallization. This issue arises from their tendency to crystallize during sintering, mainly because of a limited sintering window (called also processing window), which is defined as the difference between the crystallization onset temperature and the glass transition temperature [2]. Indeed, typical applications require thermal treatments to obtain products, such as sintered parts, scaffolds, and coatings [3,4]. In this context,

* Corresponding author.
E-mail address: valeria.cannillo@unimore.it (V. Cannillo).
[1] These authors equally contributed to this work.

https://doi.org/10.1016/j.ceramint.2024.10.135
Received 10 July 2024; Received in revised form 23 September 2024; Accepted 9 October 2024
Available online 10 October 2024

understanding the crystallization behaviour holds crucial significance, as it is widely acknowledged that crystallization can hinder or reduce bioactivity [2]. In certain cases, it may even jeopardize the stability of the implant after it has been placed in the body, given that the residual amorphous phase of the material and the crystalline phase exhibit different reactivity and dissolution rates [5]. Consequently, extensive efforts have been devoted to the identification of BG compositions with broader sintering windows, exemplified by formulations like 13–93, Bio_MS, and BGMS10 [6–8]. Among these glasses, Bio_MS (46.1 mol% SiO_2, 31.3 mol% CaO, 5 mol% Na_2O, 2.6 mol% P_2O_5, 5 mol% MgO, 10 mol% SrO) has exhibited an exceptionally high crystallization temperature (T_C) while showcasing outstanding biological performance [7]. These distinct properties are attributed to the lower content of alkaline elements and the presence of magnesium (Mg) or strontium (Sr) in the BG composition, recognized for their positive biological effects and their ability to modify thermal and mechanical properties [9–12]. In particular, Mg is regarded as functioning both as a network former and as an intermediate oxide [13,14]. It acknowledged that Mg decreases the glass transition temperature (T_G) of BGs [11,15] due to the lower strength of Si-O-Mg bond compared to Si-O-Si bond. Moreover, Mg doping can influence mechanical properties [16–18] because of its higher ionic field strength [18]. Additionally, Mg-doped BGs present optimal biocompatibility, osteogenic and cell differentiation effects [19,20], despite a possible reduction in hydroxyapatite precipitation *in vitro* on the material, compared to the case of undoped BGs [21]. On the other hand, Sr is recognized for improving apatite formation [22], while still demonstrating optimal biological and cyto-differentiation properties [23]. The effects of Sr on mechanical and thermal properties remain, however, a subject of debate [24–26].

As previously stated, numerous studies have explored the individual role of Mg and Sr in BGs behaviour. Despite the recognized beneficial effects of Mg and Sr doping on both physical and biological properties [7,8], a significant gap in the literature remains regarding systematic studies on co-doping with Mg and Sr in silicate BG composition and corresponding thermal treatments. Considering this knowledge gap, our research focuses on a set of BGs to elucidate on the non-trivial relationships between composition, sintering, crystallization, and biological responses. The chosen reference BGs for this investigation include two widely known commercial variants, namely 45S5 and S53P4. Additionally, the study considers a patented BG known as Bio_MS, distinguished by its unique composition, which includes Mg and Sr among other elements. Furthermore, our study extends its exploration by introducing doped versions of the commercial BGs. Specifically, Mg and Sr are introduced as substitutes for sodium (Na). This research focuses on two interconnected aims. The primary goal is to investigate the impact of sintering and crystallization on BGs. Simultaneously, it aims to assess how doping, specifically with ions such as Mg and Sr, influences the processes of sintering and crystallization, and the biological response of these BGs.

2. Materials and methods

2.1. Preparation of the bioactive glass

This study aims to comprehensively investigate and characterize the effects of thermal treatment on the physical, chemical, and biological properties of BGs. The production of the glasses in this study utilized a well-established melt-quenching method, which has previously been employed for the production of other BGs [1]. High-quality raw materials in powder form (Carlo Erba Reagenti, Rodano-Milano, Italy) were accurately weighed and mixed for 2 h in a laboratory rotary mixer. The mixture was melted in a platinum crucible following this thermal treatment: heated from room temperature to 1100 °C at 10 °C/min; decarbonated at 1100 °C for 1.5 h; then heated from 1100 °C to 1450 °C at 10 °C/min and held for 1 h at 1450 °C to obtain a homogeneous melt. The molten glass was subsequently quenched in water to achieve rapid cooling, resulting in the formation of a frit. The frit was then dried at 110 °C for 12 h.

A portion of each frit was then ground in a porcelain jar and sieved to obtain powders with a particle size below 63 μm. Another portion was ground and sieved to produce granules with a grain size ranging between 250 and 500 μm. This specific grain size was chosen to optimize the *in vitro* biological response, based on insights from prior studies [2,27].

The compositions of the BGs employed for the present study, expressed in mol%, are detailed in Table 1. Please note that the MgO and SrO contents in 45S5_MS and S53P4_MS were chosen to be comparable to that of Bio_MS.

2.2. Thermal analysis

The thermal behaviour of the produced BGs, in both powder and granule form (250–500 μm), was investigated via Differential Thermal Analysis (DTA) using a Differential Thermal Analyzer (STA 429 CD, Netzsch-Gerätebau GmbH, Selb, Germany). In this analysis, 30 mg of glass were placed in a platinum crucible and heated from room temperature to 1200 °C at a rate of 20 °C/min. The DTA curve obtained allowed for the determination of characteristic temperatures of the BGs, which are the glass transition temperature (T_G), onset crystallization temperature (T_{C_onset}), and peak crystallization temperature (T_C). Additionally, a heating microscope (HM) was employed to examine the behaviour of the glass powders over a broader temperature range, from room temperature to 1600 °C, with a heating rate of 10 °C/min. This was conducted using a Misura 3.32 equipment (Expert System Solutions, Modena, Italy). The purpose of this analysis was to identify the sintering temperature (T_S) and the melting temperature (T_M) of the BGs.

2.3. Sintering behaviour

To explore the impact of temperature on sintering, the glass powders were used to create disks that underwent heat treatment for 3 h at five arbitrarily chosen temperatures: 650 °C, 750 °C, 850 °C, 950 °C, and 1050 °C. The evaluation of sintering quality was based on the observed degree of shrinkage. The process to create the green bodies involved subjecting the glass powders to uniaxial pressing at a pressure of 7 bar for 10 s. Subsequently, five green bodies of each BG were placed in a muffle furnace (AWF 13/12, Lenton - Laboratory Scientific Equipment, Randburg, South Africa) and subjected to heat treatment at the specified temperatures, employing a heating rate of 10 °C/min. Following the thermal treatment, the samples were air-cooled to reach room temperature. To assess the changes in size resulting from shrinkage, the diameters of the samples were measured using a digital calliper (LTF 327.09, LTF S.p.A., Antegnate, Italy). The temperature associated with the maximum observed shrinkage was considered the best sintering temperature (T_{BS}).

2.4. Phases analysis

To compare the impact of heat treatment on the five BG compositions, granules were subjected to heat treatment at two specific temperatures: T_C determined via DTA analysis, and T_{BS} determined as previously described. Both treatments lasted 3 h. The phase composition

Table 1
Composition in mol% of the five BGs.

Sample	SiO_2	P_2O_5	Na_2O	CaO	MgO	SrO
45S5	46.1	2.6	24.4	26.9	–	–
S53P4	53.8	1.7	22.7	21.8	–	–
Bio_MS	46.1	2.6	5	31.3	5	10
45S5_MS	46.1	2.6	9.4	26.9	5	10
S53P4_MS	53.8	1.7	7.7	21.8	5	10

of both untreated and treated granules, along with the potential formation of crystalline phases, was examined using X-Ray Diffractometry (XRD: X'Pert PRO; Panalytical, Almelo, the Netherlands). Data collection was obtained by a 2θ scan method in the range of 10–90° using Cukα X-ray line (step size: 0.017° 2θ).

2.5. Physical and mechanical properties

To determine the density of the samples treated at T_{BS}, cross-sectional analysis was conducted using image analysis techniques. The Environmental Scanning Electron Microscope (ESEM) (Quanta 2000, Fei Co., Eindhoven, Netherlands) was employed to capture images of the samples, and ImageJ software was used to assess the porosity from the images. Following the density evaluation, the mechanical properties were examined using Open Platform equipment (CSM Instruments, Peseux, Switzerland) with a Vickers indenter tip. A load of 1000 mN was applied during indentation, with a loading/unloading rate of 2000 mN/min and a hold time of 15 s. Each sample was tested at least 15 times, and the load-penetration depth curve was automatically recorded for each indentation. Young's modulus was automatically calculated using the method proposed by Oliver and Pharr [28].

2.6. SBF testing

The assessment of the bioactivity of the BG granules involved their immersion in Simulated Body Fluid (SBF), following the Kokubo protocol [29,30]. Specifically, 1.5 g of BG granules were submerged in 50 mL of SBF and incubated at 37 °C for durations of 3, 7, and 14 days. The pH of the solution was monitored, and the SBF was replaced every 48 h. The starting pH of the solution was 7.4 as specified by the Kokubo protocol [30,31]. After each time interval, the granules were collected via filtration and washed with distilled water. At the end of the test, the samples were air-dried at room temperature for 24 h.

The apatite-forming ability of both heat treated and untreated glasses was assessed using XRD and micro-Raman spectroscopy (LabRAM, Horiba Jobin-Yvon, Villeneuve D'Aseq, France). The spectrometer was equipped with a diode laser operating at a wavelength of 632.8 nm and delivering 20 mW of power to the sample. The scattered photons were dispersed using a grating monochromator with a resolution of 1800 lines/mm and then captured by a CCD camera. An optic with a 100× Ultra Long Working Distance (ULWD) objective was utilized. The spectral data were collected through a series of 15 acquisitions, each lasting 20 s. Lastly, the microstructure of the samples was examined using ESEM equipped with X-ray energy dispersive spectroscopy (EDS) (Inca, Oxford Instruments, UK), conducted under low-vacuum conditions (~0.5 Torr).

2.7. Cytotoxicity according to ISO 10993

To prepare the eluates, BGs were incubated with Dulbecco Modified Eagle Medium (DMEM) (Thermo Fisher Scientific, MA, USA) at 37 °C for 16 h, as recommended by ISO 10993–12 procedures [32]. Eluates were sterilised using 0.22 μm filters (Merck-Life Science, Darmstadt, Germany).

Balb/3T3 embryonic mouse fibroblast cell line (American Type Culture Collection, ATCC) is widely used for testing cytotoxicity. Cells were seeded at a density of 10^3 cells/well in 96-well plates and cultured in DMEM supplemented with 10 % foetal bovine serum, 1 % penicillin-streptomycin and 1 % non-essential amino acids (Thermo Fisher Scientific). After 24 h, the culture medium was replaced with eluates at different concentrations (i.e., 100 %, 50 %, 25 % and 12.5 %). Negative and positive controls were set using the culture medium only, or the culture medium plus 0.1 % sodium dodecyl sulphate (SDS, Merck-Life Science), respectively. After additional 24 h, cell morphology was evaluated under a phase-contrast microscope (DIAPHOT-TMD, Nikon, Japan) and cytotoxicity was assessed with the MTT assay as recommended by the ISO 10993–5 protocol (Biological Evaluation of Medical Devices - Part 5: Tests for In Vitro Cytotoxicity). Briefly, tetrazolium salts (1 mg/mL in DMEM) were added to the cell culture and incubated at 37 °C in humidified atmosphere (95 % air and 5 % CO_2) for 2 h, then the medium was removed, and 200 μL of dimethyl sulphoxide were added to each well to dissolve formazan crystals. The optical density (O.D.) was measured at 540 nm using a multiplate reader (Multiskan FC, Thermo Fisher Scientific). Data were expressed as percentage of O.D. values of metabolically active living cells in cultures with the presence of eluates compared to cells incubated in the absence of eluates set at 100 %. Blank absorbance was represented by the medium alone. MTT assay was performed in sextuplicate.

2.8. Cell viability and cell adhesion

Human dermal fibroblasts (HDFs) from adult donors (Cat #C-013-5C, Invitrogen, USA) were cultured and maintained according to Boraldi et al. [33]. BGs were sterilised by UV light and placed into 96-well ultra-low adhesion plates (Cat #3474, Corning, USA) without washing. HDFs were seeded onto BG ($1.5x10^5$ cells/50 mg of BG) and cultured in standard cell culture conditions for 7 days. The culture medium was changed every two days. At different times of culture (i.e., 1h, 4 and 7 days), cell viability and cell morphology were evaluated by MTT assay and by optical digital microscopy (VHX-7000, Keyence, Japan), respectively. For cell morphology, the cells were fixed with 20 % cold methanol and stained with 0.5 % crystal violet [34]. Area (total area of each cell), perimeter, aspect ratio (the ratio between the major and minor axis of a cell) were evaluated using the Image software (v.1.53t) on approximately 80 cells/sample.

2.9. Cell growth

For cell growth assessment, 12-well plates (Falcon) were prepared with a cell density of 6.0×10^4 cells/well in 1 mL of complete DMEM or in 1 mL of 100 % eluate obtained from BG 45S5 T_{BS} (for the preparation of the eluate see paragraph 2.7). Cells were cultured for 7 days with changes of the medium (DMEM or eluate) on the fifth day of culture. Cell counts were performed at day 1, 4 and 7 after seeding using the Neubauer chamber.

2.10. Statistical analysis

One-way analysis of variance (ANOVA) was used for multiple comparisons and a Tukey post-hoc test was applied. Statistical analyses were performed using GraphPad Prism 8.0 software (San Diego, CA). Values are reported as mean ± standard deviation (SD). Differences were considered significant for $p < 0.05$.

3. Results and discussion

3.1. Thermal analysis

Fig. 1(A–E) presents the DTA curves of the BGs, acquired while heating at a rate of 20 °C/min using fine powders (<63 μm). The observed glass transition temperatures T_G for 45S5 and S53P4, measuring 520 °C and 530 °C, respectively, are consistent with data documented in existing literature [35–39]. Similarly, the data obtained for Bio_MS aligns with the analysis conducted in prior research [7], thereby establishing a foundational platform for comparing with other MS-doped BGs. However, it's important to note that while the findings concerning the crystallization temperature T_C of 45S5 and Bio_MS align with literature [7,35–37,39], the data for S53P4 contradicts existing studies. Specifically, the recorded T_C is 648 °C, unlike the range found in other studies, which report a T_C between 730 °C and 805 °C [38,40]. This discrepancy could potentially be attributed to the granulometry used for the DTA analysis or the heating rate employed during

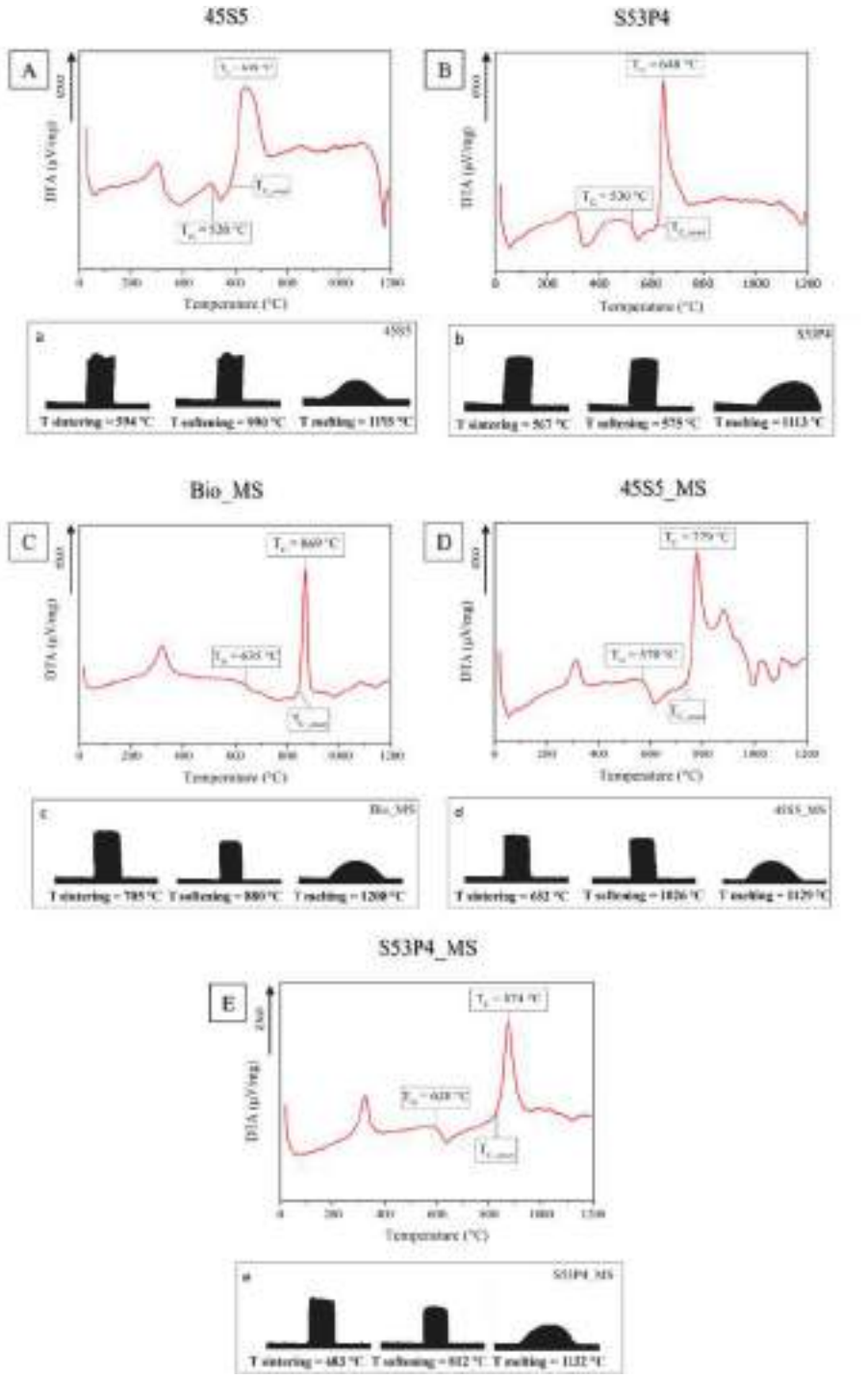

Fig. 1. DTA and HM analyses of: (A) 45S5, (B) S53P4, (C) Bio_MS, (D) 45S5_MS and (E) S53P4_MS. The characteristic temperatures T_G, T_{C_onset} and T_C are shown on the DTA curves.

evaluation. Further DTA analyses on BG coarse powder showed the well-known effect of grain size on the thermal behaviour of the glasses. Comparative data between powders and granules for each composition are provided in the Supplementary Materials (Fig. S1), highlighting an increase in T_C with increasing grain size, consistent with literature findings [41].

Fig. 1 also illustrates the results of the HM analysis, delineating the sintering, softening (marking the initiation of BG collapse owing to viscous flow), and melting temperatures of the samples. The data highlighted that the "MS" samples exhibit higher sintering temperature compared to their parent glass, with Bio_MS showing to have the highest sintering temperature. However, this analysis alone does not comprehensively reveal the optimal sintering conditions for BGs but rather indicates the temperature at which the glass begins to contract. Therefore, additional studies were conducted to explore BGs behaviour under various sintering conditions.

3.2. Sintering behaviour

Table 2 showcases the results obtained from a shrinkage assessment conducted at different temperatures, highlighting the best sintering temperature T_{BS} in green. For 45S5, as observed by Bretcanu et al. [35]

Table 2
Values of shrinking (expressed as percentages) of the BG disks after heat treatment for 3 h at different temperatures. The highlighted values represent the highest value of shrinkage measured for each BG.

Shrinkage % at the respective temperatures					
Sample	650 °C	750 °C	850 °C	950 °C	1050 °C
45S5	2 % (±0.48)	2 % (±0.91)	3 % (±0.52)	7 % (±0.96)	10 % (±1.21)
S53P4	10 % (±0.68)	7 % (±1.81)	7 % (±0.96)	8 % (±1.51)	–
Bio_MS	0 % (±0.40)	13 % (±0.55)	13 % (±1.24)	10 % (±0.62)	10 % (±1.30)
45S5_MS	13 % (±0.62)	14 % (±0.96)	13 % (±1.44)	9 % (±1.02)	9 % (±0.35)
S53P4_MS	8 % (±1.33)	14 % (±1.08)	11 % (±1.30)	7 % (±2.41)	14 % (±1.07)

and Lefebvre et al. [42], the sintering process reveals two distinct stages: an initial phase followed by a more prolonged and marked stage. Densification initiates at 650 °C during the first step, while the second densification phase starts at 950 °C, peaking at 1050 °C. The shrinkage associated with the first step measures approximately 2 %, whereas a higher shrinkage rate of around 10 % was recorded during the subsequent phase of densification. Remarkably, the T_{BS} identified in this study aligns with findings reported by Chen et al. [43]. In the case of the S53P4, the glass exhibited the highest level of shrinkage at 650 °C, suggesting this temperature as potentially ideal for the sintering process. However, this observation contradicts other studies that identified 720 °C as the optimal sintering temperature [38,44]. It is worth noting that in these studies, the determination of the optimal sintering temperature relied on manually testing the fragility of BG-scaffolds produced at different temperatures. It is noteworthy to mention that the S53P4 samples encountered difficulty in being sintered at 1050 °C due to glass softening, thus making the measurement of shrinkage impossible in those conditions. Regarding Bio_MS, its identified T_{BS} aligns with the findings of a previous study [7]. Similarly, for other MS-doped bioactive glasses, the maximum densification occurred at 750 °C, diverging from the sintering temperatures suggested by the HM analysis, which were 50–100 °C lower. Notably, Bio_MS, 45S5_MS, and S53P4_MS also exhibit superior sinterability compared to commercial BGs.

Table 3 summarizes the characteristic temperatures found for the five glass compositions. The processing window, defined as the difference between the temperature of crystallization onset and T_G, and the sinterability parameter ($S_C = T_{C\_onset} - T_{BS}$) are reported as well. The sinterability parameter S_C of a glass is an estimate of its sintering ability versus its crystallization trend. In particular, if T_{C_onset} is lower than the sintering temperature, then $Sc < 0$ and the glass is likely to crystallize before it can sinter; this usually results in non-optimal densification. On the other hand, if $Sc > 0$, the glass can sinter without crystallizing, and thus compaction is promoted.

It is crucial to highlight the beneficial effect of reducing the alkaline content and doping with Mg-Sr on the sintering behaviour of BGs. This leads to increased sample shrinkage and widens the processing window of doped BGs. This observed trend likely results from various factors contributing to higher T_C: lower Na content in doped BGs, potentially reducing glass network mobility [45], enhanced stability of MgO-doped glasses due to MgO's inhibitory effect on crystallization [9], higher entropy supporting the preservation of the BG network's amorphous structure, and the possible augmentation of flow viscosity owing to the presence of Sr^{2+} [46].

Table 3
Characteristic temperatures of the five BGs, obtained through various techniques: T_G glass transition temperature; T_{C_onset} onset crystallization temperature; T_C peak crystallization temperature; T_{BS} best sintering temperature; processing window (T_{C_onset} - T_G), and sinterability parameter ($S_C = T_{C\_onset}$ - T_{BS}).

	T_G	T_{C_onset}	T_C	T_{BS}	Processing window	S_C
45S5	520 °C	560 °C	638 °C	1050 °C	40 °C	<0
S53P4	530 °C	615 °C	648 °C	650 °C	85 °C	<0
Bio_MS	635 °C	830 °C	869 °C	750 °C	195 °C	80 °C
45S5_MS	570 °C	740 °C	779 °C	750 °C	170 °C	<0
S53P4_MS	620 °C	810 °C	874 °C	750 °C	190 °C	60 °C

3.3. Phases analysis

Fig. 2 presents XRD analysis results of 45S5 and 45S5_MS subjected to different heat treatments: untreated and heated at T_C and T_{BS} for 3 h. Our analysis indicates that after post-thermal treatment, the primary crystalline phase identified is combeite ($Na_4Ca_4Si_6O_{18}$, JCPSD no. 01-079-1086). This aligns with previous studies on the crystallization of 45S5 [47,48], although other crystalline phases have also been identified [49,50]. The influence of Mg and Sr on the crystallization behaviour must be considered. Notably, the doped glass exhibits a lower degree of crystallization compared to pure 45S5. This finding suggests the potential for significant control over the crystallization of doped BG, enabling regulation of the crystalline-to-amorphous BG ratio. Such control could potentially dictate the mechanical and bioactive properties of the BG [51]. It is important to note that the analysed samples do not display any peak associated with crystalline phases of Mg and/or Sr, as confirmed in previous studies [52]. Fig. 3 displays the XRD analysis of the five BG compositions treated at T_{BS} for 3 h. The analysis indicated the formation of combeite (Na4Ca4Si6O18, JCPSD no. 01-079-1086) in thermally treated S53P4, as reported elsewhere [53]. The impact of Mg-Sr doping and the concurrent reduction in the alkaline element content on crystallization is readily apparent, as the doped BGs exhibit minimal to no crystallization. Specifically, a lower tendency to crystallize is observed in Bio_MS and S53P4_MS. This tendency could be attributed to their lower sodium content, resulting in reduced diffusion coefficients and slower rates of crystal growth [54].

3.4. Physical and mechanical properties

Fig. 4 presents the cross-section images of BG samples heat treated at their respective T_{BS}. The diagram in Fig. 5 illustrates the density obtained through image analysis. Notably, all examined BG compositions demonstrate exceptional density levels, surpassing 95 %. While Bio_MS exhibits higher shrinkage compared to the commercial BGs, its density is slightly lower. This discrepancy in density may be attributed to larger pore dimensions observed in Bio_MS compared to those of other BG compositions. Regarding other MS-doped BG compositions, the higher shrinkage aligns with the increased density found by image analysis, confirming the superior sinterability of these BG compositions.

The chart depicted in Fig. 6 provides the results of the mechanical properties of the BGs analysed in the present study. Consistently, the hardness values obtained for 45S5 and S53P4 align with established literature sources [55,56]. However, there is a noticeable scarcity of studies specifically investigating the hardness of Bio_MS or the MS-doped compositions, although the results presented here indicate higher values compared to other Mg or Sr doped BGs [12,57]. The impact of Mg and Sr on the hardness of 45S5_MS is clearly discernible from the data, as it results higher than the reference commercial BG. In contrast, data suggest a marginal reduction in hardness within the S53P4_MS sample. This distinct behaviour might be linked to the different Mg-Sr/Si ratios. Notably, Mg exhibits dual characteristics as both a network modifier and a network former [58], potentially resulting in the formation of quite strong Mg-O-Si bond [57] or the weakening of the overall glass network [15]. In the case of Sr-doped BGs, the potential weakening of the glass structure is attributed to the small but significant expansion of the glass network as a consequence of the substitution of Ca by Sr [59]. This expansion occurs due to the larger size

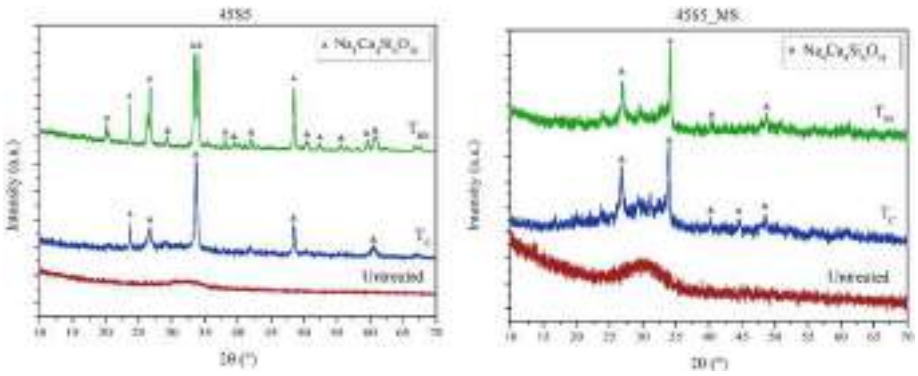

Fig. 2. XRD spectra of 45S5 and 45S5_MS samples in different conditions: untreated (red curve), after heat treatment at T_C for 3 h (blue curve), and after heat treatment at T_{BS} for 3 h (green curve). (For interpretation of the references to colour in this figure legend, the reader is referred to the Web version of this article.)

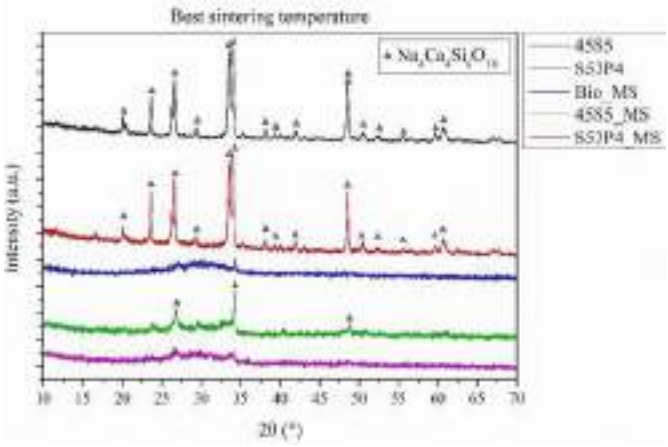

Fig. 3. XRD spectra of the five BGs after heat treatment at T_{BS} for 3 h.

of the Sr^{2+} cation compared to Ca^{2+}. The impact of doping on the elastic modulus (E) appears to be minimal, aligning with findings similar to those reported by Sharifianjazi et al. [57]. Nonetheless, direct comparisons with existing literature present challenges due to the scarcity of studies specifically addressing the mechanical properties of bulk BG. It's important to note that the presence of residual pores and variations in powder granulometry might significantly impact the mechanical properties of sintered BGs [12,60]. This aspect warrants further investigation and consideration in interpreting the presented results.

Finally, it is important to note that BGs are intrinsically brittle materials and, therefore, in load bearing applications, are used as coatings, e.g. on metallic prostheses. In this case, besides the fact that the BGs are thermally treated, it is important to pay attention to the mismatch of the coefficient of thermal expansion of the BG and the metallic substrate. In fact, due to such mismatch, thermal stresses may arise [61,62].

3.5. SBF assesment

Fig. 7(A–C) compares the effects of different composition on the pH

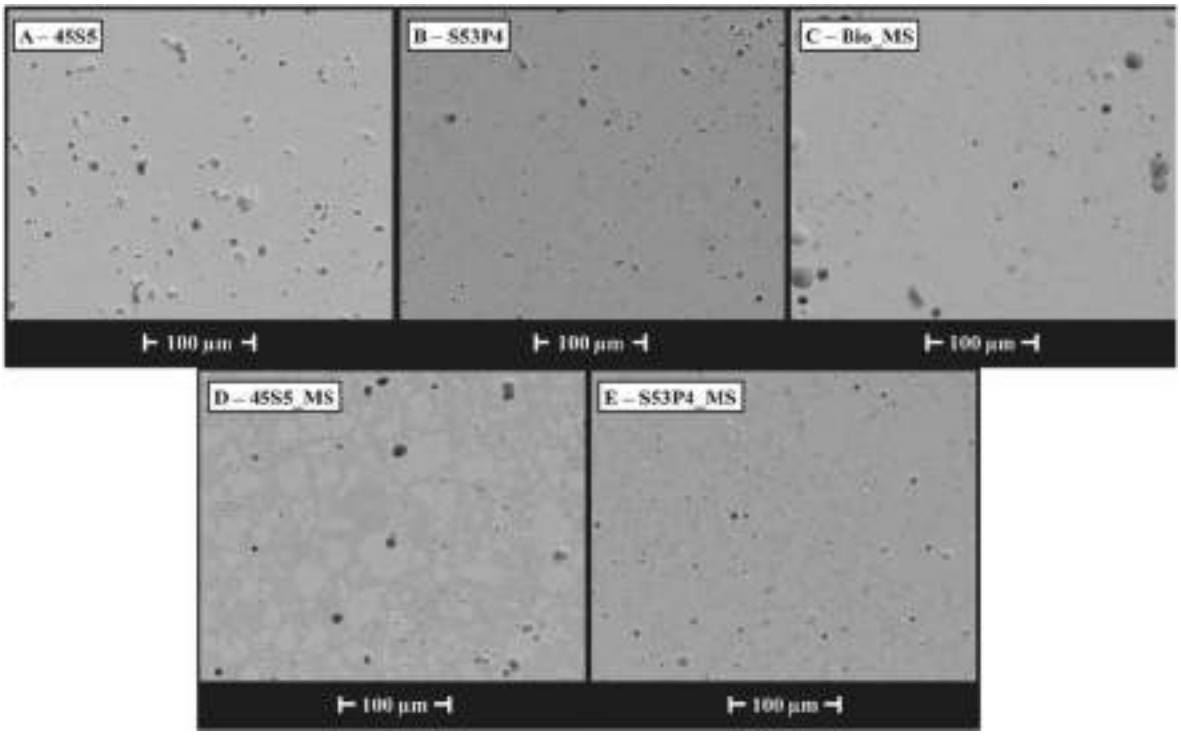

Fig. 4. (A–E). SEM micrographs of the cross-sections of the five BGs disks samples heat treated at their respective T_{BS}.

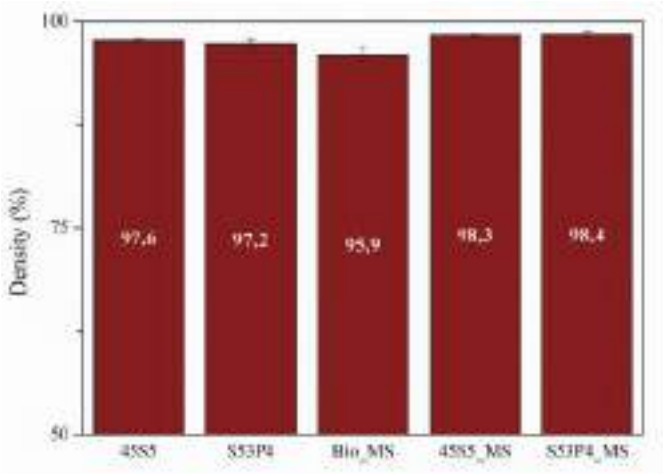

Fig. 5. Calculated density of the BG disks after sintering at T_{BS}. Results were obtained analysing the cross-section images.

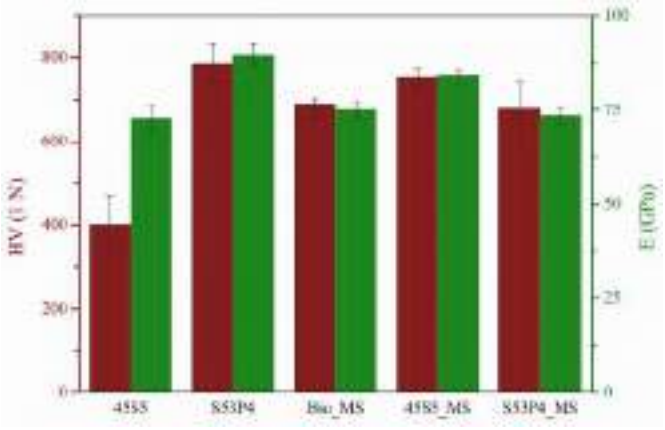

Fig. 6. Mechanical properties (specifically, microhardness and elastic modulus) of the sintered BG disks.

of the SBF, to show the pH variation in the same heat treatment conditions. Results show that the heat treatment can influence the reactivity of BG compositions, as reported in other studies [63]. In the same figure, the optimal pH range for tissue regeneration has been added [64]. Indeed, it has been demonstrated that a weakly alkaline environment, up to pH 8, can enhance osteogenic activities and promote antibacterial effects without toxic effects on cells [65–68]. Taking this into account, a delayed and lower reactivity of BG can be seen positively, considering the need for a controlled, slower reaction while retaining bioactivity. This result was achieved with BGs doped with Mg and Sr and a lower alkali content. Moreover, these findings are consistent with the literature, which reports that Mg and Sr influence the reactivity of BG *in vitro* [11,69]. Furthermore, it can be seen how the doped samples heat treated at T_{BS} are able to maintain a lower pH than the samples heat treated at T_C. This finding is promising for glasses containing Mg and Sr, since it may point to a greater propensity of these compositions for the application as sintered BGs, allowing a simpler and more successful development of sintered parts.

The *in vitro* bioactivity of a BG, specifically its ability to induce an HA precipitation, can be assessed using Raman spectroscopy. The results of the analysis are depicted in Fig. 8, illustrating the Raman spectra of untreated granules of 45S5, S53P4, Bio_MS, 45S5_MS and S53P4_MS after soaking in SBF for 7 days. Analogous results were obtained from the analyses of crystals grown on the surfaces of heat-treated BGs. A representative Raman spectrum acquired on the precipitates of a heat-treated sample is reported in the Supplementary Materials (Fig. S2). Examination of the spectra reveals the presence of typical peaks attributable to *in vitro* precipitated HA: one around 430 cm^{-1}, another at 590 cm^{-1}, and a prominent narrow peak at about 960 cm^{-1}. These peaks can be attributed to the bond stretching of the $(PO_4)^{3-}$ groups [71,72]. Moreover, a peak at 1070 cm^{-1}, related to the stretching of the carbonate groups, confirms that the HA formed is carbonated, as reported in the literature [73]. These observations apply to all untreated samples following a 7-day immersion in SBF, thus confirming their bioactivity. However, the kinetics of HA deposition on the surface of the granules varies among the samples. The diminished reactivity of BGs containing Mg and Sr, which may ultimately lead to less HA precipitation, can be observed through the analysis of the Raman spectra. An example of this behaviour is illustrated in Fig. 9(A and B), which shows the Raman spectra of untreated S53P4 and S53P4_MS granules, both as-fritted and after soaking in SBF for 3 and 7 days. Examination of the spectra of both

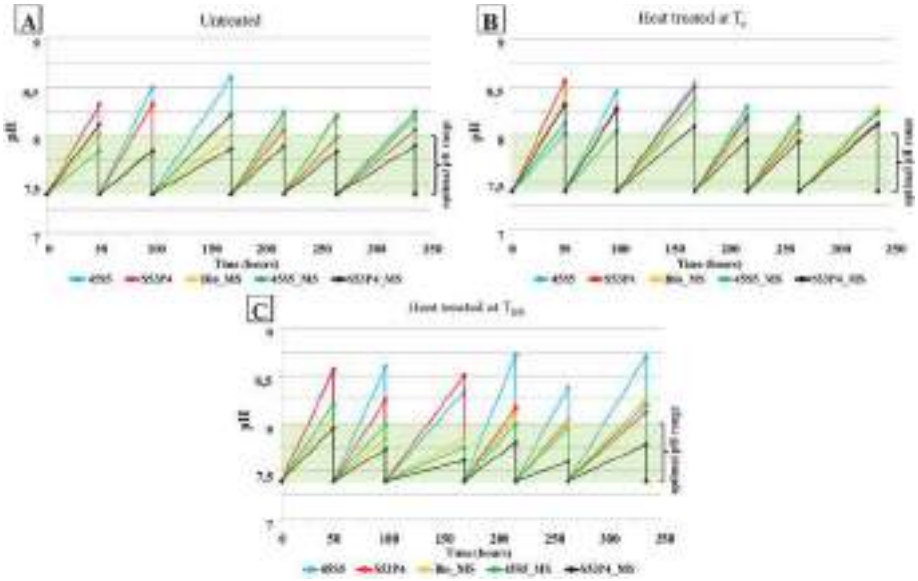

Fig. 7. (A–C). pH variation induced by the untreated samples (A), and by the heat-treated samples at T_c (B), and T_{BS} (C). The green area represents the optimal pH for osteoblast activity [70]. (For interpretation of the references to colour in this figure legend, the reader is referred to the Web version of this article.)

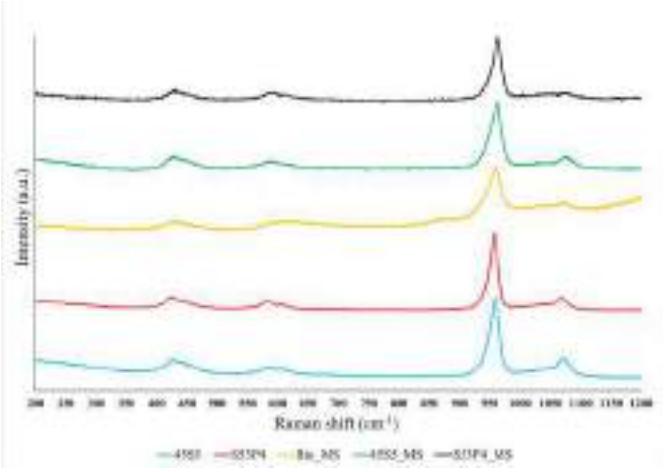

Fig. 8. Raman spectra acquired on untreated BG granules after immersion for 7 days in SBF.

samples before immersion in SBF reveals a broad peak at 625 cm^{-1}, corresponding to the vibration of the Si-O-Si silicate groups [74]. Additionally, a broad peak around 940 cm^{-1} is due to the vibration of the $(PO_4)^{3-}$ groups present in the BG structure [75]. After 3 days S53P4_MS exhibits result similar to those at time 0 day (Fig. 9B), whereas the spectrum of S53P4 showed peaks at 430 cm^{-1}, 590 cm^{-1}, 960 cm^{-1} and at 1070 cm^{-1} (Fig. 9A). Similar results were obtained for untreated 45S5 and 45S5_MS granules soaked in SBF; the Raman spectra observed for Bio_MS granules closely resemble those seen in glasses that contain strontium and magnesium (data not shown).

The surfaces of the samples after immersion in SBF were observed using SEM. A qualitative chemical analysis was conducted by means of EDS. Figs. 10 and 11 present the results of the SEM/EDS analysis of the surfaces of some representative BGs after soaking in SBF. Specifically, Fig. 10(A–D) shows the SEM/EDS of the S53P4 (A-B) and S53P4_MS (C-D) samples after 3 days of soaking in SBF solution, respectively. Results show that the surface of S53P4 is covered by spherical particles with a cauliflower-like structure, which is typical of the HA formed *in vitro*. However, these kinds of deposits cannot be detected on the surface of the S53P4_MS samples, apart from local formations, supporting the previous hypothesis of the slower reactivity of this composition compared to its counterpart that does not contain strontium and magnesium. Additional considerations can be made based on the EDS analysis. In fact, in the EDS spectrum of S53P4_MS, a pronounced presence of silicon is observed, indicative of the formation of a superficial silica gel layer. The gel formation is an essential part of the reactions leading to the precipitation of HA and dehydrates after extraction from SBF, resulting in the typical

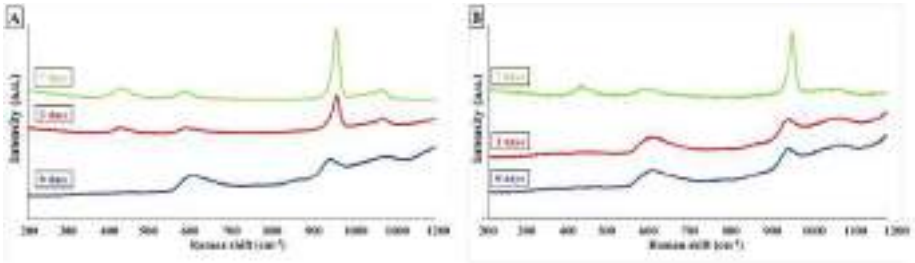

Fig. 9. (A–B). Raman spectra acquired on S53P4 (A) and S53P4_MS (B) untreated granules after immersion for different times in Simulated Body Fluid.

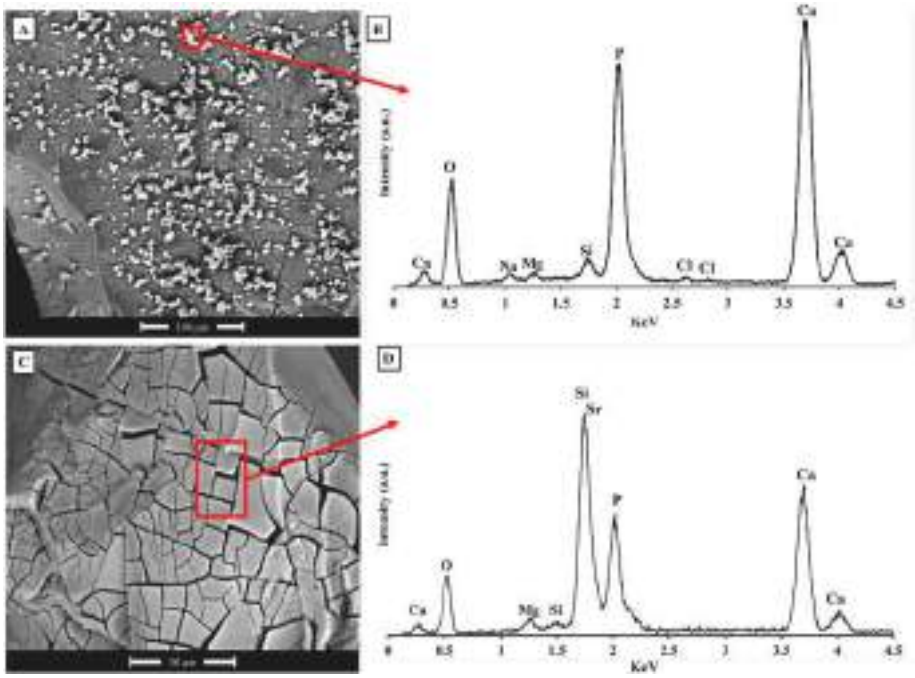

Fig. 10. (A–D). (A) SEM micrograph of S53P4 sample after 3 days of soaking in SBF, and (B) EDS analysis of the highlighter (red) area in micrograph (A). (C) SEM micrograph of S53P4_MS sample after 3 days of soaking in SBF, and (D) EDS analysis of the highlighter (red) area in micrograph (C). (For interpretation of the references to colour in this figure legend, the reader is referred to the Web version of this article.)

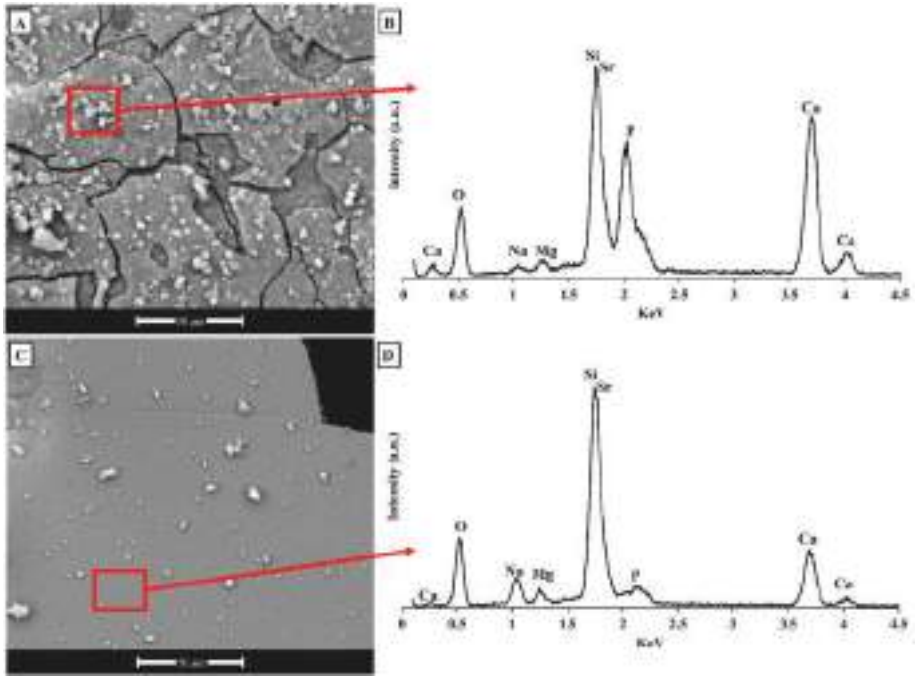

Fig. 11. (A–D). (A) SEM micrograph of 45S5_MS sample, heat treated at T_C after 7 days of soaking in SBF, and (B) EDS analysis of the highlighter (red) area in micrograph (A). (C) SEM micrograph of S53P4_MS sample, heat treated at T_C after 7 days of soaking in SBF, and (D) EDS analysis of the highlighter (red) area in micrograph (C). (For interpretation of the references to colour in this figure legend, the reader is referred to the Web version of this article.)

cracked surface visible in Fig. 10 (C) [75,76]. Furthermore, the EDS analysis shows an increase in the phosphorus peak, attributable to the formation of localized precipitates rich in phosphorus and calcium, precursors of HA [77]. It can therefore be concluded that the HA formation process on S53P4_MS is at a less advanced stage. The presence of small amounts of magnesium and chlorine on the S53P4 sample (Fig. 10 (A)) is likely due to the deposition of salts precipitating from the SBF, as reported by the literature [78]. Similar observations can be made for the 45S5 and 45S5_MS samples. Regarding Bio_MS, after 3 days, it tends to behave *in vitro* like the other glasses containing magnesium and strontium (data not shown).

Fig. 11(A–D) shows the EDS analysis for the 45S5_MS (A-B) and S53P4_MS (C-D) samples after heat treatment at T_C and 7 days of immersion in SBF. This analysis aims to highlight the different effects of Mg and Sr, as well as a lower alkali content, on two different BG compositions. On the surface of the 45S5_MS (Fig. 11 (A)) some globular precipitates are clearly visible. EDS analysis confirms that these precipitates have high concentrations of Ca and P, supporting the hypothesis of HA formation on the surface (further confirmed by Raman investigation – data not shown). Fig. 11(C and D) shows the results of S53P4_MS after heat treatment at T_C. Some HA precipitates are visible, but the surface is less covered compared to the 45S5_MS samples, indicating lower bioactivity of the S53P4_MS sample, even after 7 days of exposure to SBF. Nevertheless, both experimental compositions are bioactive after heat treatment at T_C.

These results are further supported by Fig. 12, which illustrates SEM images comparing the temporal evolution of the surfaces of untreated BG samples containing Mg and Sr after 3, 7, and 14 days of soaking in SBF. It is evident that, after 3 days, the samples containing Mg and Sr present few to none deposits with the typical morphology of HA, thus confirming, as previously discussed, that the Mg/Sr doped compositions are less reactive than the undoped counterparts [69]. However, after 14 days of immersion, all surfaces are covered with a layer of HA, confirming the bioactivity of all BGs and the abundant deposition of HA on their surfaces after 14 days of immersion.

Finally, Fig. 13(A–J) presents SEM images of BGs, both non-heat-treated and heat-treated at T_C, after 14 days of soaking in SBF. These images demonstrate that all the samples are highly bioactive after 14 days in SBF, as they exhibit HA globular precipitates on their surfaces. This further supports the high reactivity of these BGs, even after thermal treatment.

3.6. Biological assessment

3.6.1. Cytotoxicity test

MTT test is routinely used to evaluate the possible cytotoxicity of biomaterials and other medical devices, before conducting more detailed analyses on more complex experimental models [79]. MTT is a yellow tetrazolium salt that is metabolized by mitochondrial dehydrogenases leading to the formation of purple formazan crystals [80]. The intensity of the purple colour is representative of the number of metabolically active cells capable of converting MTT, as an indicator of cell proliferation, viability and cytotoxicity. According to ISO 10993–5, samples are considered noncytotoxic when the cell viability is never below the threshold value of 70 % compared to cells cultured in the absence of eluates (set ay 100 %) (Fig. 14) Balb 3T3 fibroblasts were incubated with different concentrations (*i.e.,* 100 %, 50 %, 25 % and 12.5 %) of eluates from the different BGs untreated and treated at different temperatures (Fig. 14). Only the positive control (*i.e.,* cells in DMEM + SDS) shows cytotoxicity, while all tested BGs, regardless of their different composition, heat treatment and eluates' concentration, do not exhibit any cytotoxic effect.

3.6.2. Viability and adhesion of human dermal fibroblasts grown onto BGs

BGs have several well-known clinical applications in dental or orthopaedic areas as scaffolds promoting bone regeneration [81,82]. Data reported in previous sections have already highlighted the ability of BGs to favour the deposition of hydroxyapatite due to ion exchange on the BGs' surface, even in the absence of cells.

Therefore, we aimed at widening the spectrum of possible applications of BGs also in the field of soft connective tissue repair, given the clinical impact of defective wound healing [83]. In this study we have evaluated cell viability and the interactions between BGs and human dermal fibroblasts (HDFs) in primary culture as a prototype of soft

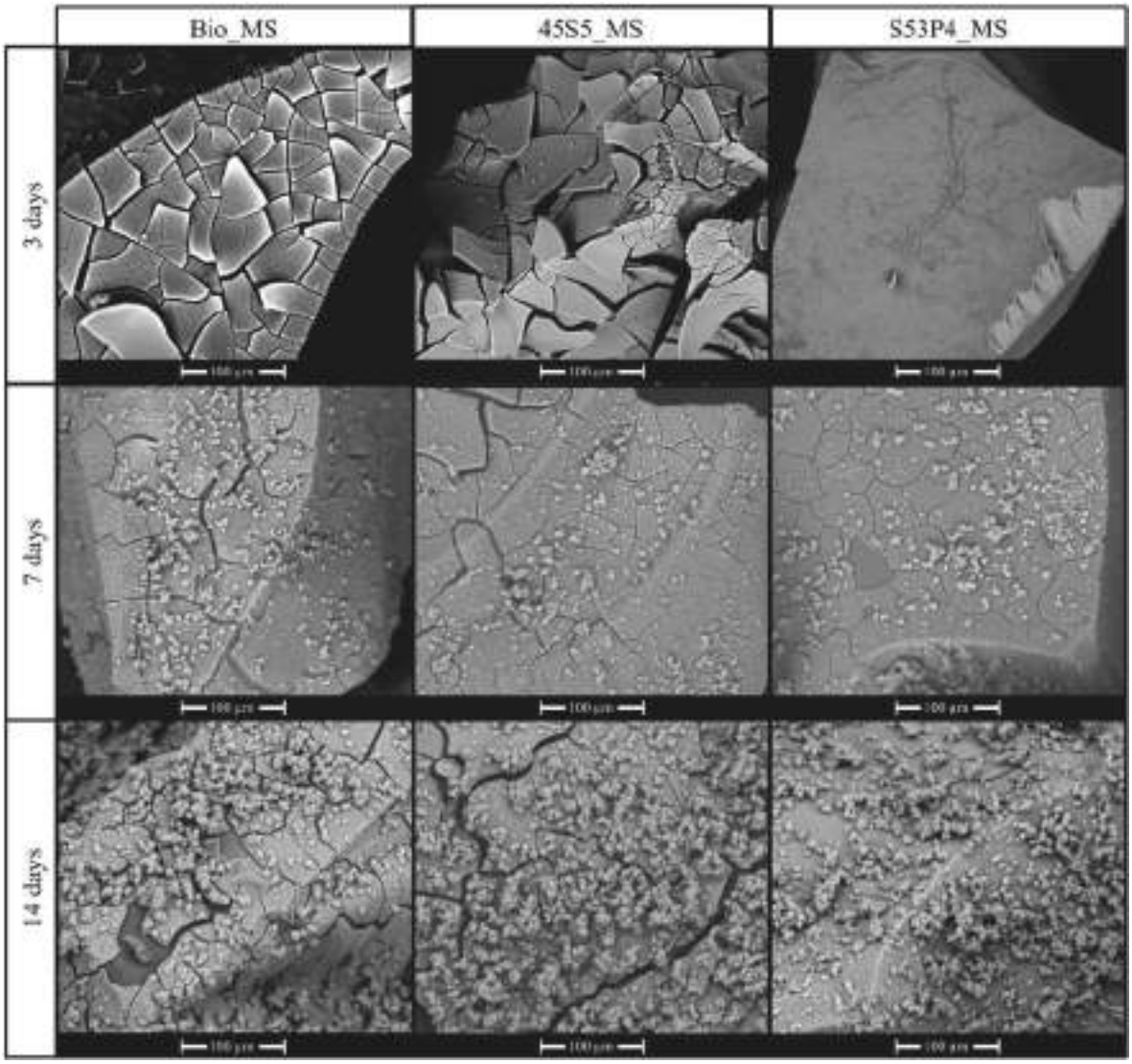

Fig. 12. Grid of SEM micrograph of Bio_MS, 45S5_MS and S53P4_MS untreated samples after 3, 7 and 14 days of soaking in SBF.

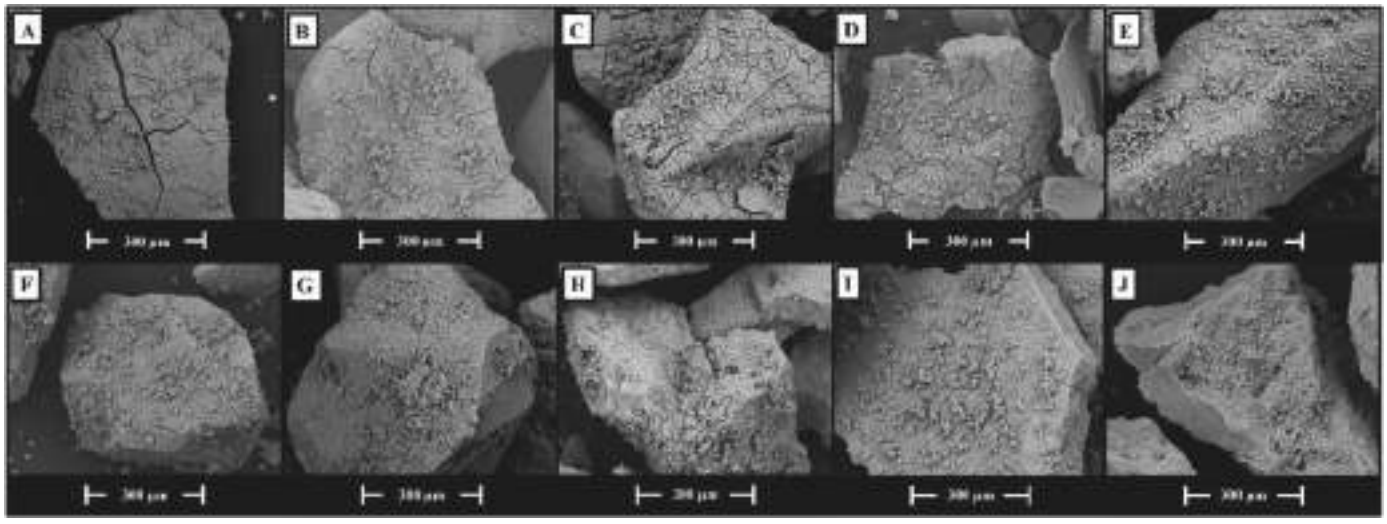

Fig. 13. SEM micrographs of: 45S5 (A), S53P4 (B), Bio_MS (C), 45S5_MS (D), and S53P4_MS (E) untreated granules after 14 days of soaking in SBF, and 45S5 (F), S53P4 (G), Bio_MS (H), 45S5_MS (I), and S53P4_MS (J) granules heat treated at T_c after 14 days of soaking in SBF.

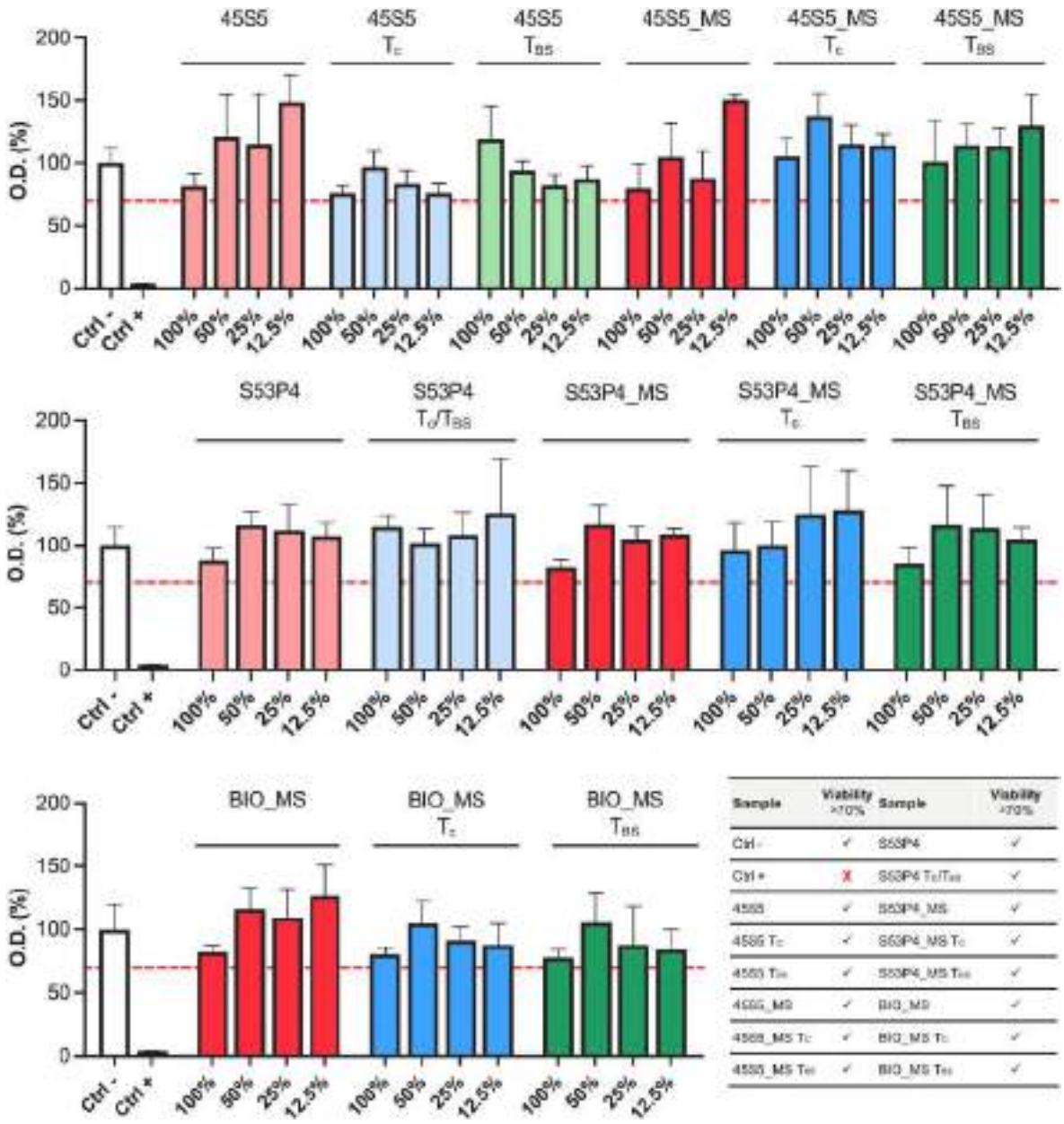

Sample	Viability >70%	Sample	Viability >70%
Ctrl -	✓	S53P4	✓
Ctrl +	✗	S53P4 Tc/TBS	✓
45S5	✓	S53P4_MS	✓
45S5 Tc	✓	S53P4_MS Tc	✓
45S5 TBS	✓	S53P4_MS TBS	✓
45S5_MS	✓	BIO_MS	✓
45S5_MS Tc	✓	BIO_MS Tc	✓
45S5_MS TBS	✓	BIO_MS TBS	✓

Fig. 14. ISO 10993–5 cytotoxicity test. The viability of the Balb 3T3 cell line was evaluated by the MTT test after 24 h in the absence (DMEM, Ctrl-) or in the presence of different concentrations (100 %, 50 %, 25 % and 12.5 %) of eluates from the BGs. The positive control was represented by cells treated for 24 h with DMEM plus 0.1 % SDS (Ctrl +). Optical density (O.D.) from cells cultured in DMEM was set at 100 %. The dotted line represents the threshold value of 70 %, compared to Ctrl-, that, according to the ISO 10993-5 guidelines, is required to demonstrate the absence of cytotoxicity. Values represent the mean ± SD of two independent experiments. (T_C = crystallization temperature; T_{BS} = best sintering temperature).

connective tissue mesenchymal cells producing the different components of the extracellular matrix [84,85].

Since, we have previously demonstrated that a novel patented BG, Bio_MS [86], due to the integration of Mg and Sr (MS) in its composition, has promising applicative perspectives and improved thermal properties, we included in our biological evaluations also two commercially available BGs (i.e., 45S5 and S53P4) modified with the addition of MS.

Furthermore, to better investigate the behaviour of cells directly interacting with BGs, HDFs were seeded on the surface of BGs and cell viability, adhesion properties and morphology of cells at different time points, up to 7 days, were evaluated.

Data reported in Fig. 15 for Bio_MS indicate that cell viability is affected by the treatment at $\mathbf{T_C}$ but not at $\mathbf{T_{BS}}$. To be noted, however, that reduction of cell viability at 4 and 7 days, compared to 1h, was always less than 20 %.

Morphological observations and morphometrical analyses performed on HDFs grown on Bio_MS at different temperatures of treatment demonstrated good adhesion properties (see Fig. 16). A consistent number of cells adhered to the surface of BGs independently of treatments. As expected, cells were round after 1 h but appeared well spread and elongated after 4 and 7 days from seeding. At 7 days, fibroblasts on Bio_MS T_c appeared slightly, but significantly smaller compared to Bio_MS, suggesting that changes in the characteristics of the BG's surface may influence the way cells interact with the BG. In this case, the bioactivity of Bio_MS treated at T_{BS} is not influenced by the sintering temperature. Indeed, as demonstrated in previous studies, one of the advantages of the Bio_MS formulation is the wide processing window with regards to heat treatment. Developing formulations that can be

Time	BIO_MS	BIO_MS T_C	BIO_MS T_{BS}
1 h	**100±5**	80±4	94±5
4 d	82±10§	69±11	83±13
7 d	85±7§	67±8	95±14

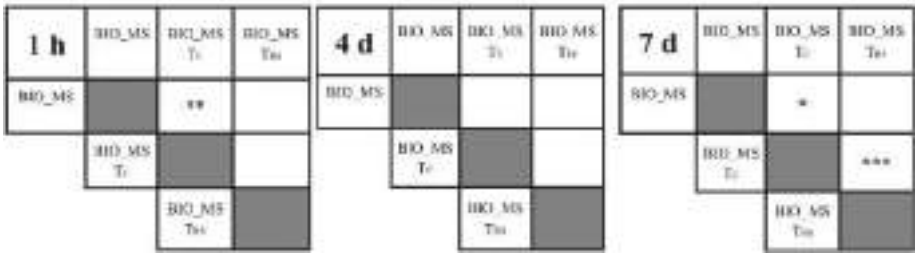

Fig. 15. Cell viability of human dermal fibroblasts grown for 1 h (1h), 4 and 7 days (4d and 7d) on Bio_MS untreated or treated at different temperatures (T_C = crystallization temperature; T_{BS} = best sintering temperature).
Data are expressed as mean values ± SD. Values obtained with Bio_MS at 1h without any treatment were set at 100 %.
§p value < 0.05 of 4 or 7 days *vs* 1h in the same experimental condition; *p value < 0.05, **p value < 0.01, ***p value < 0.001 between BGs untreated or treated at different temperatures at the same time point.

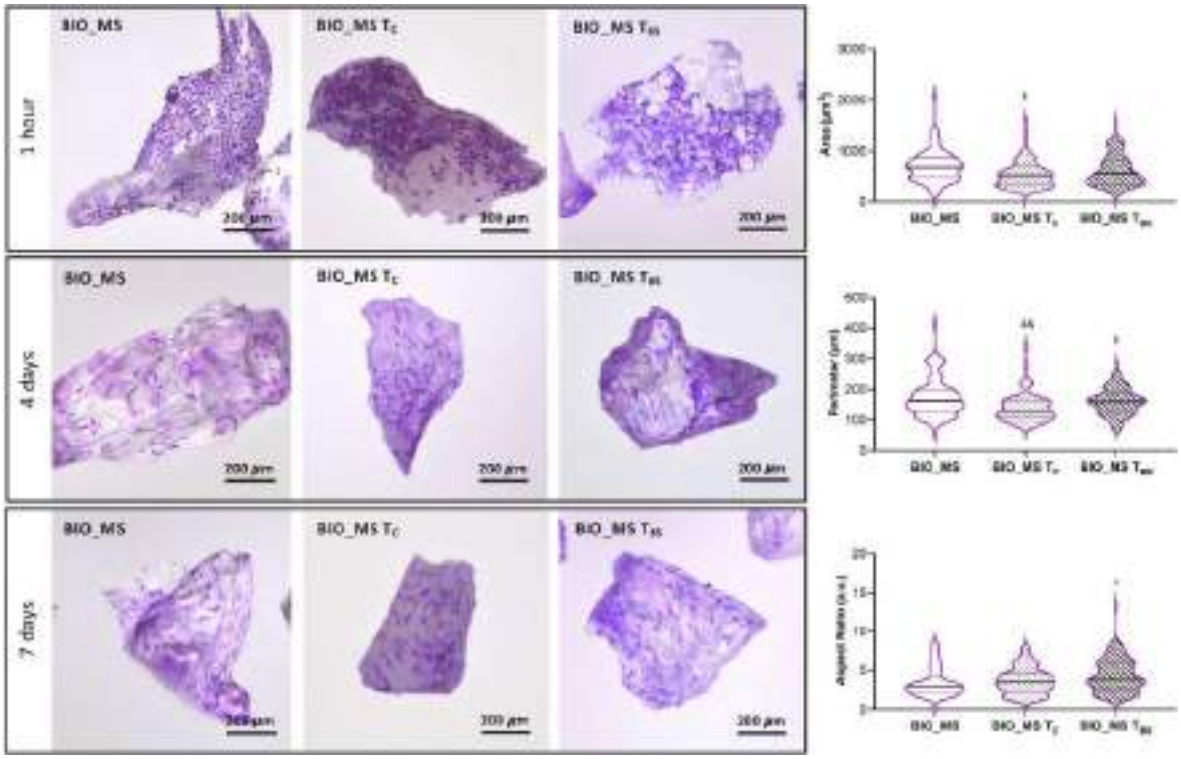

Fig. 16. Representative images of HDFs seeded for 1 h, 4 and 7 days on Bio_MS untreated and treated at different temperatures (T_C = crystallization temperature; T_{BS} = best sintering temperature). Violin plot representing area, perimeter and aspect ratio evaluated after 7 days of culture. & $p < 0.05$, && $p < 0.01$ MS T_C vs MS; $ $p < 0.05$ MS T_{BS} vs MS T_C; ° $p < 0.05$ MS T_{BS} vs MS.

sintered without forming crystals and that are able to maintain good cell viability is an essential requirement for biomedical perspectives [87]. Since thermal treatments are necessary for the manufacturing of composite materials, porous scaffolds or coatings [87], Bio_MS treated at T_{BS} emerges as a possible candidate capable of maintaining high biocompatibility even after treatment at high temperatures.

The same type of analyses described for Bio-MS, were performed on BGs used as reference standards and on the same commercial BGs also supplemented with MS.

Fig. 17 indicates that cell viability is progressively reduced on 45S5 without addition of MS and that these effects are particularly evident after treatment at T_{BS}. Data seem in contrast with the well-known properties of this BG, that represents the gold standard for implants, for supporting structures to be used in bone tissue regeneration [88] or

Time	45S5	45S5 T_C	45S5 T_{BS}	45S5_MS	45S5_MS T_C	45S5_MS T_{BS}
1 h	**100±11**	93±1	91±2	112±14	114±8	98±8
4 d	56±10§§§§	93±20	9±1§§§§	83±15§§§	75±5§§§§	93±9
7 d	67±10§§§	69±13§§	8±2§§§§	96±10§	104±20§§	113±12§§

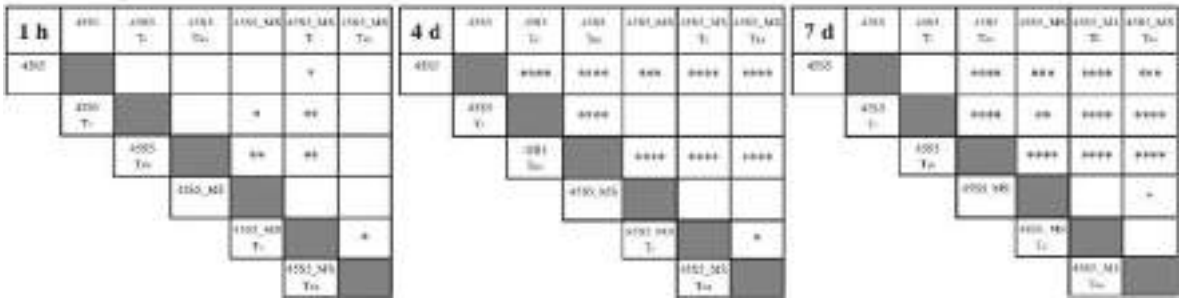

Fig. 17. Cell viability of human dermal fibroblasts grown for 1 h (1h), 4 and 7 days (4d and 7d) on 45S5 and 45S5_MS untreated or treated at different temperatures (T_C = crystallization temperature; T_{BS} = best sintering temperature). Data are expressed as mean values ± SD. Values obtained with 45S5 without any treatment at 1 h were set at 100 %.
§p value < 0.05, §§p value < 0.01, §§§p value < 0.001, §§§§p value < 0.0001 of 4 or 7 days vs 1h in the experimental condition; $^{\#}$p value < 0.05, $^{\#\#}$p value < 0.01 of 7 vs 4 days; *p value < 0.05, **p value < 0.01, ***p value < 0.001, ****p value < 0.0001 between BGs untreated or treated at different temperatures at the same time point.

for the re-mineralization of tooth enamel [89,90]. However, its applicability and usability in the regeneration of loose connective tissues or in wound repair have been poorly investigated [91–93]. Within this context, it is worth mentioning that most of the data in the literature concerns the use of bone-related cells. For instance, 45S5 does not interfere with osteoblast viability, since these cells are well adapted to the extra- and intracellular alkalinization exerted by the BG [94]. Interestingly, a previous study by Day and coworkers [95], using a fibroblast cell line (208F) cultured on surfaces coated with 45S5, demonstrated a reduced cell proliferation depending on the time of culture (48 and 72 h) and/or on the concentration (0.01–0.2%wt/vol) of 45S5. In the light of these data we can suggest that HDFs in primary culture, compared to other cells, may have different interactions with the BG and that even local changes in the pH, without any pre-treatment of the BG (e.g., with serum components, simulated body fluid - SBF, or with adhesive glycoproteins) [96], can influence cell adhesion [97] and cell proliferation, possibly mimicking *in vitro* what can happen *in vivo*, i.e. when the BGs are implanted.

It is well known that the adsorption of proteins on the BG is influenced by numerous factors, both external (e.g., pH and temperature) and internal (e.g., surface charges and topography of the BG surface) [98].

Interestingly, MS-doped BG showed a significantly improved cell viability, effects being also independent of temperatures. At 7 days of culture, the viability of cells grown on doped BGs was 1greater than on BGs. Noteworthy data obtained with the 45S5_MS T_{BS} vs 45S5 T_{BS} since addition of MS completely abolished the cytotoxic effect of the thermal treatment. In doped-BGs cell viability showed a general decrease at day 4 and an increase at day 7. These data suggest that 45S5_MS, regardless of treatment, induces an initial selection within the cell population in favour of a subpopulation capable of better adapting to the microenvironment, as already observed in the literature [99].

The better performance observed for the doped 45S5 is associated with the addition of MS. This result is not surprising, as it has been already demonstrated that the addition of Mg to BGs promotes the adhesion of bone-derived cells [100]. Indeed, previous studies demonstrated that Mg promotes cell adhesion favouring the synthesis of collagen type I, vitronectin, fibronectin and the activation of kinases associated with focal adhesions in osteoblasts [101,102] as well as in human fibroblasts [103]. Furthermore, also Sr can act as an inducer of cell adhesion and proliferation, as shown on BGs subjected to treatments at temperatures that can compromise the bioactivity of the biomaterial [25], and can promote both osteogenesis and angiogenesis when added to BG nanoparticles [10]. Furthermore, Sr can maintain an optimal pH in the surrounding environment, thus ensuring good cell viability [104].

The interactions between cells and BGs were also assessed by evaluating the morphology of HDFs grown up to 7 days on 45S5 and 45S5_MS at different temperatures. Morphometric analyses were also performed at 7 days to quantitate differences in the spreading of the cells.

HDFs adhered well on all BGs at 1h, although, as expected, they are still round. Over time in culture, cells acquired a more elongated shape except for 45S5 T_{BS}. Due to the low number of cells on 45S5 T_{BS}, morphometric analyses on these samples were not performed.

MS-doped BG allowed to maintain the number of adhered cells that exhibited a more spread morphology compared to cells on 45S5 (Fig. 18) confirming the beneficial role of MS addition.

Since cell viability and adhesion were severely affected on 45S5 T_{BS}, we wanted to test if the observed effects were due to the release of specific components affecting cell behaviour or if the cells negatively responded to changes of the surface of the BGs. Therefore, HDFs were cultured on standard multiwell plates in the presence of DMEM or of 100 % eluates from 45S5T_{BS}. Fibroblasts, in the presence of 100 % 45S5 T_{BS} eluates, exhibited good proliferation capabilities (see Fig. 19).

Data demonstrate that the reduced cell viability observed with 45S5 T_{BS} is not due to cytotoxic components released by the BG but could be linked to modifications of the microstructure of the BG following heat treatment, as suggested by previous studies [105]. The operating conditions adopted during the sintering process for the consolidation of the powders, can modify the compositional and structural characteristics of the BG, which in turn influence mechanical and biological properties. Indeed, it has been observed that, as the temperature increases, the surface of 45S5 goes from smooth to wrinkled with consequences on the bioactivity of the BG [105]. Therefore, cell viability is not influenced by ions and/or toxic components released by the BG, but more likely by changes occurring on the surface of the BG after treatment at sintering

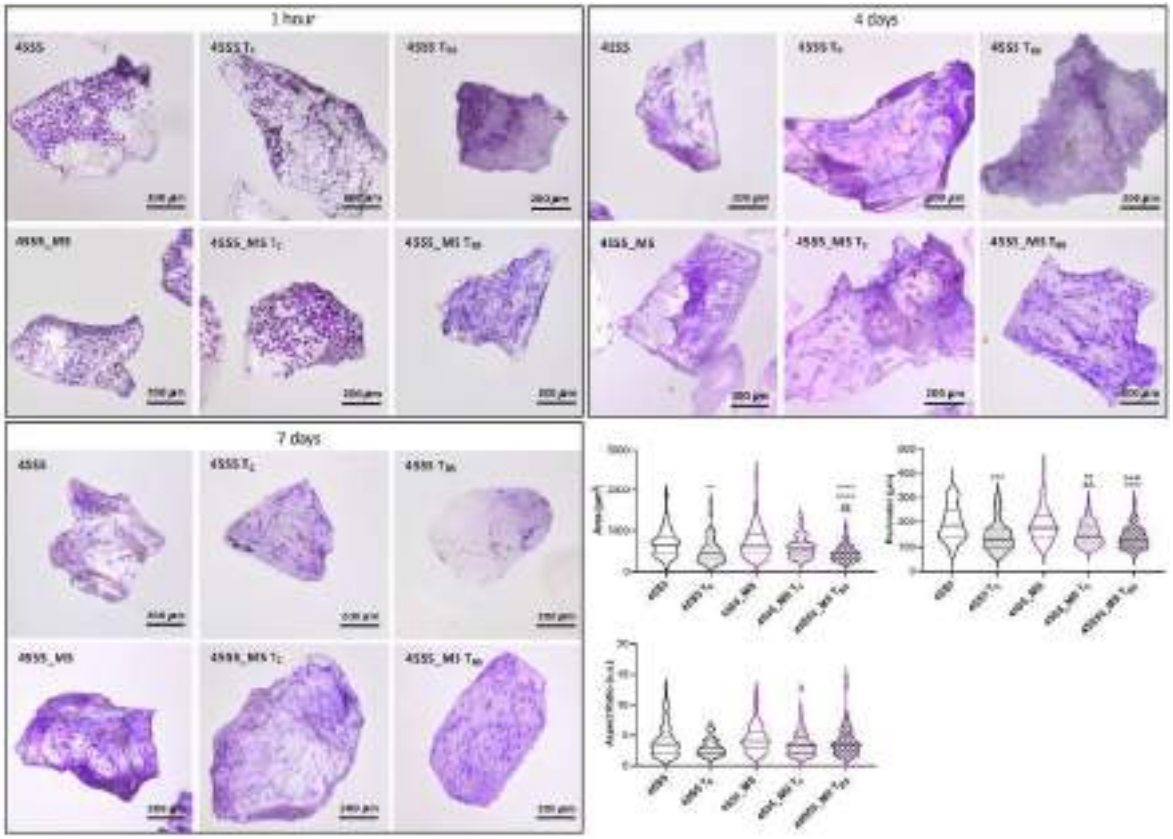

Fig. 18. Representative images of HDFs seeded for 1 h, 4 and 7 days on 45S5 and 45S5_MS untreated and treated at different temperatures (T_C = crystallization temperature; T_{BS} = best sintering temperature). Violin plot representing area, perimeter and aspect ratio evaluated after 7 days of culture. **p < 0.01, ***p < 0.001, ****p < 0.0001 all conditions vs 45S5; $^{\&}$p < 0.05, $^{\&\&}$p < 0.01 MS T_C vs MS; $^{\circ}$p < 0.0001 MS T_{BS} vs MS; $^{\$\$}$p < 0.01 MS T_{BS} vs MS T_C.

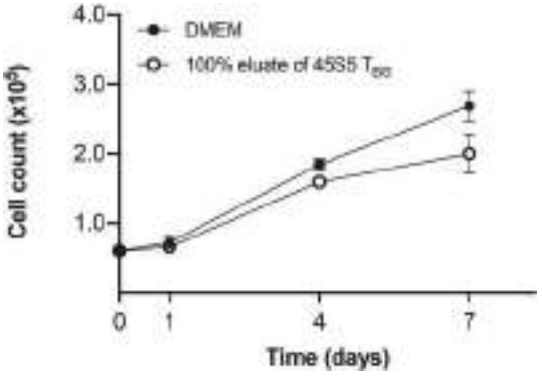

Fig. 19. Cell proliferation. HDF were grown in DMEM or in DMEM+ 100 % eluate from 45S5 T_{BS} ($\mathbf{T_{BS}}$= best sintering temperature) and cell number evaluated at different time points after seeding. There are no significant differences between the two experimental conditions. Data are expressed as mean values ± SD.

temperature.

In Fig. 20 data show the viability of cells grown on the S53P4, that was developed and mainly used in clinical applications related to bone healing, vascularization, and cartilage repair [106,107]. Although there are several data in the literature related to the effect of BG S53P4 on bone-derived cells (osteoblasts and osteoclasts) [108–110], to our knowledge, there are no studies on the use of dermal fibroblasts.

In the present study, cell viability is progressively reduced on the BG both without any heat treatment or at temperatures T_C/T_{BS}. Similarly, to 45S5_MS, also S53P4_MS showed significantly improved cell viability, effects being independent on temperatures.

The interactions between cells and S53P4 BGs were assessed by evaluating the morphology of HDFs grown up to 7 days on the BGs. Morphometric analyses were also performed at 7 days to quantitate differences in the spreading of cells.

When HDFs were grown on S53P4, after 1h, cell behaviour was similar to that on 45S5. By contrast after 4 and 7 days, the number of adhered cells was reduced on BG treated at T_C/T_{BS}, thus underlining the effect of treatment on adhesion and cell viability of cells in contact with BGs. On the contrary, S53P4_MS exhibited nicely spread and typically elongated HDFs. Data, once more, clearly demonstrated the positive effect of the addition of Mg and Sr to the BG (Fig. 21).

Finally, to better evaluate cell viability of HDFs in the different experimental conditions, BGs were compared to each other based on their formulation, regardless of the heat treatment. In particular, cell viability was evaluated on BGs without heat treatment (NHT), on BGs treated at crystallization temperatures (Tc) and on BGs treated at best sintering temperatures (T_{BS}). The cell viability data were compared with results of the non-thermally treated 45S5, considered the gold standard of BGs currently on the market [88].

In group NHT, cell viability on 45S5_MS and Bio_MS was higher than on standard BG (45S5) (Fig. 22).

In group Tc, cell viability was significantly higher for all BGs with MS compared to the same BGs without MS (Fig. 22).

In group T_{BS} it clearly emerges that the addition of MS to the BGs significantly increased the cell viability of HDFs compared to formulations without MS. Furthermore, cell viability was similar among the three MS-containing BGs (Fig. 22).

Time	S53P4	S53P4 T_C/T_{BS}	S53P4_MS	S53P4_MS T_C	S53P4_MS T_{BS}
1 h	**100±11**	86±8	127±11	110±5	125±9
4 d	82±6§§	79±14	104±11§	82±10§§	107±11
7 d	67±14§§§§	55±5§§§§^^^^	79±10§§§§^^^^	97±10	120±19

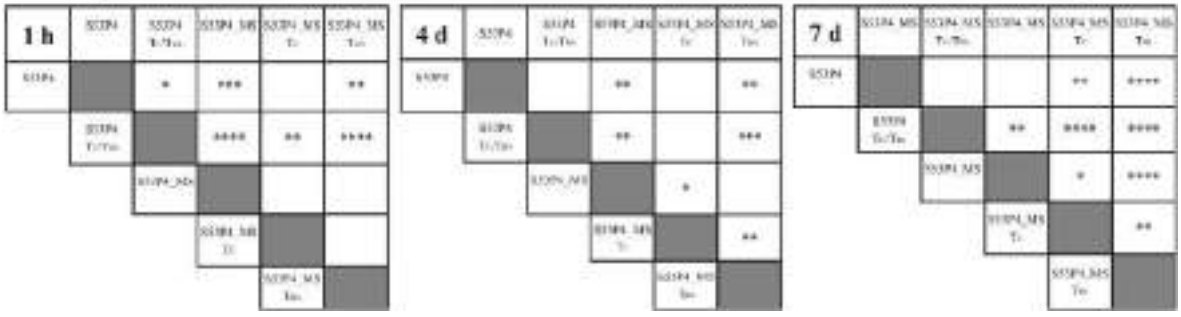

Fig. 20. Cell viability of human dermal fibroblasts grown for 1 h (1h), 4 and 7 days (4d and 7d) on S53P4 and S53P4_MS untreated or treated at different temperatures (T_C = crystallization temperature; T_{BS} = best sintering temperature). Data are expressed as mean values ± SD. Values obtained with S53P4 were set at 100 %. §p value < 0.05, §§p value < 0.01, §§§p value < 0.001, §§§§p value < 0.0001 of 4 or 7 days vs 1h in the same experimental condition; #p value < 0.05, ##p value < 0.01 of 7 vs 4 days; *p value < 0.05, **p value < 0.01, ***p value < 0.001, ****p value < 0.0001 between BGs untreated or treated at different temperatures at the same time point.

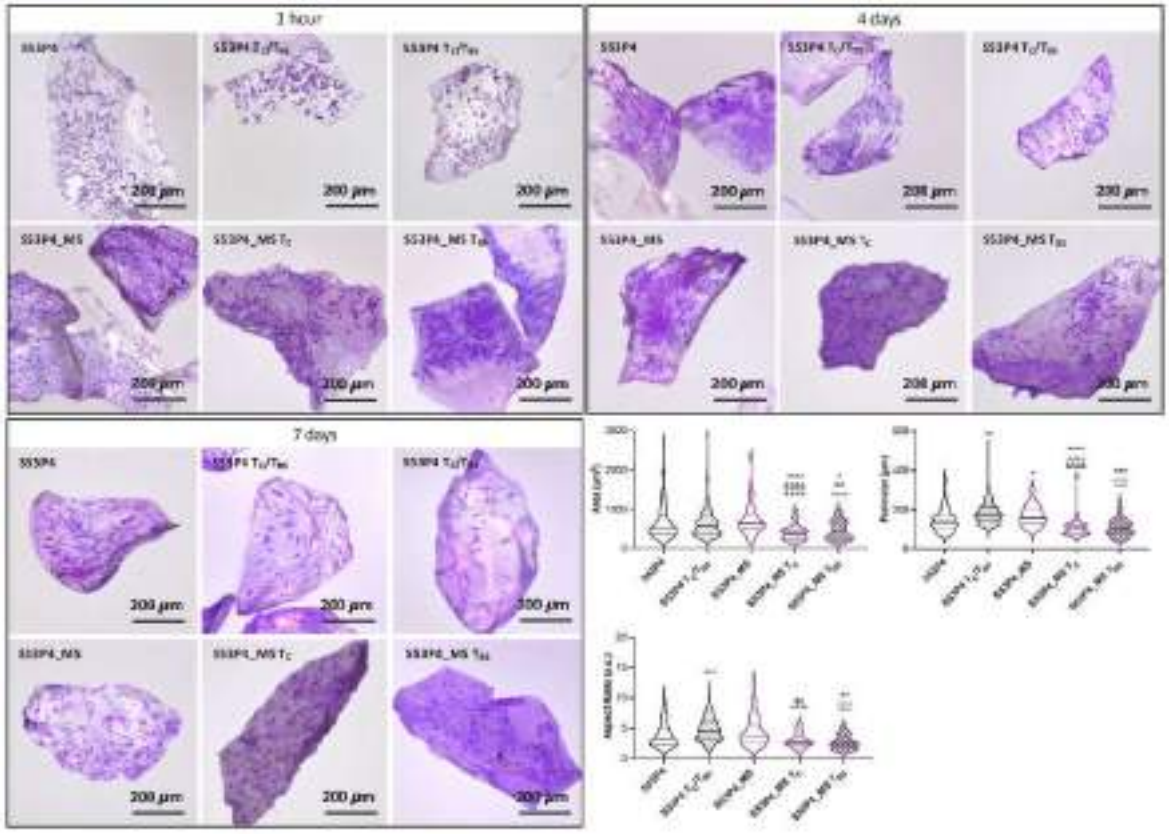

Fig. 21. Representative images of HDFs seeded for 1 h, 4 and 7 days on S53P4 and S53P4_MS untreated and treated at different temperatures (T_C = crystallization temperature; T_{BS} = best sintering temperature). Violin plot representing area, perimeter and aspect ratio evaluated after 7 days of culture. *p < 0.05, **p < 0.01, ***p < 0.001, ****p < 0.0001 all conditions vs S53P4; && p < 0.01, &&&& p < 0.0001 MS T_C vs MS; ° p < 0.0001 MS T_{BS} vs MS; ++++ p < 0.0001 T_C/T_{BS} vs MS T_C; ^^ p < 0.01, ^^^^ p < 0.0001 T_C/T_{BS} vs MS T_{BS}.

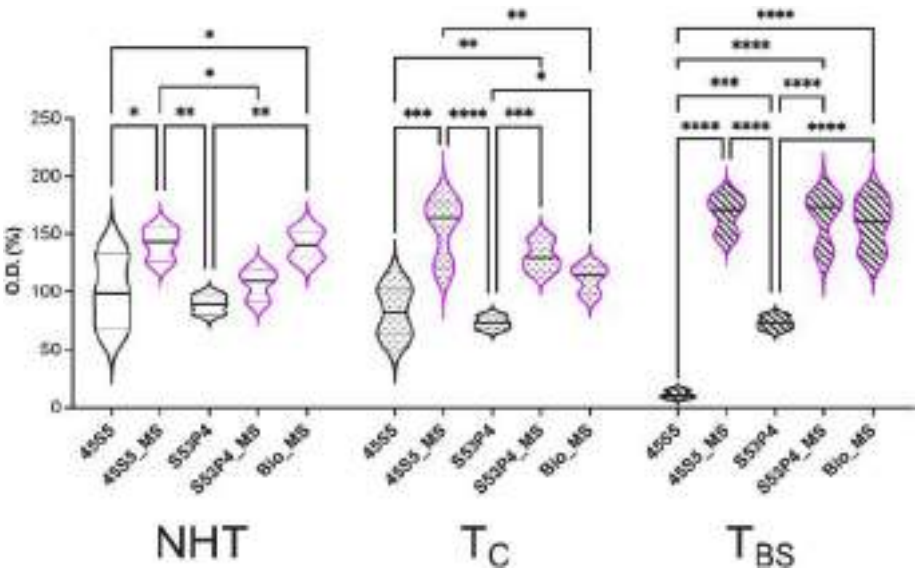

Fig. 22. Violin plot representation of the cell viability of HDFs grown on non-heat-treated (NHT) or heat-treated bioglasses (BGs) for 7 days. T_C = crystallization temperature; T_{BS} = best sintering temperature. Values of optical density (O.D.) obtained with 45S5 at 7 days were set to 100 %. *p value < 0.05; **p value < 0.01; ***p value < 0.001; ****p value < 0.0001.

4. Conclusions

The results show several positive effects of the substitution of Mg^{2+} and Sr^{2+} ions in the "MS" BG compositions. Specifically:

- Both T_G and T_C show a significant increase in value in MS-doped BGs, while also showcasing a wider sintering window. This may allow for low temperature sintering of the BGs.
- Heat treating the MS-doped BGs resulted in quasi-amorphous or low-crystallites-containing structures. Lower temperatures were able to create sintered BG samples while retaining a mostly amorphous structure. Densification was also higher for the MS-doped BGs.
- 45S5_MS showed better mechanical properties after sintering heat treatment compared to sintered 45S5. Meanwhile, S53P4_MS showed mechanical properties similar to other BGs in this study.
- The MS-doped BGs resulted bioactive after SBF testing, although they presented slower reaction kinetic. This can also prove beneficial, as the pH of the solution increased less compared to the undoped BGs.
- A good interaction between bioglasses and HDF suggesting their possible use in soft connective tissues, in addition to what has already been demonstrated for bone and cartilaginous tissues.
- Treatment at high temperatures can modify the surface of BGs with consequences on cellular adhesion, as highlighted in the case of 45S5 T_{BS}.
- Bio_MS, a recently formulated BG, confirms its excellent biocompatibility also using HDF.
- The integration of MS in two BGs which, in the standard formulation, are already widely used for orthopaedic and dental applications, further improves the performance of BGs;
- The positive effect of MS is particularly evident when BGs are treated at T_C and T_{BS}.

CRediT authorship contribution statement

Devis Bellucci: Writing – review & editing, Methodology, Data curation, Conceptualization. **Alessia Mazzilli:** Writing – original draft, Investigation, Data curation. **Andrea Martelli:** Writing – original draft, Investigation, Data curation. **Francesco Gerardo Mecca:** Writing – original draft, Investigation, Data curation. **Susanna Bonacorsi:** Writing – original draft, Investigation, Data curation. **Francesco Demetrio Lofaro:** Writing – original draft, Investigation, Data curation. **Federica Boraldi:** Writing – review & editing, Methodology, Data curation, Conceptualization. **Daniela Quaglino:** Writing – review & editing, Supervision, Methodology, Funding acquisition, Data curation, Conceptualization. **Valeria Cannillo:** Writing – review & editing, Supervision, Methodology, Funding acquisition, Data curation, Conceptualization.

Declaration of competing interest

The authors declare the following: the bioactive glass Bio_MS (in granules) was patented (Italian patent No 102019000002229 dated February 15, 2019).

Acknowledgements

Valeria Cannillo, Daniela Quaglino and Francesco Gerardo Mecca acknowledge financial support from the PNRR MUR project ECS_00000033_ECOSISTER.

Appendix A. Supplementary data

Supplementary data to this article can be found online at https://doi.org/10.1016/j.ceramint.2024.10.135.

References

[1] L.L. Hench, R.J. Splinter, W.C. Allen, T.K. Greenlee, Bonding mechanisms at the interface of ceramic prosthetic materials, J. Biomed. Mater. Res. 5 (1971) 117–141, https://doi.org/10.1002/JBM.820050611.
[2] J.R. Jones, Review of bioactive glass: from hench to hybrids, Acta Biomater. 9 (2013) 4457–4486, https://doi.org/10.1016/J.ACTBIO.2012.08.023.
[3] F. Baino, E. Verne, Glass-based coatings on biomedical implants: a state-of-the-art review, Biomedical Glasses 3 (2017) 1–17.
[4] J. Henao, C. Poblano-Salas, M. Monsalve, J. Corona-Castuera, O. Barceinas-Sanchez, Bio-active glass coatings manufactured by thermal spray: a status report, J. Mater. Res. Technol. 8 (2019).
[5] O.P. Filho, G.P. Latorre, L.L. Hench, Effect of crystallization on apatite-layer formation of bioactive glass 45S5, J. Biomed. Mater. Res. 30 (1996), https://doi.org/10.1002/(SICI)1097-4636(199604)30:4<509::AID-JBM9>3.0.CO;2-T.
[6] M. Brink, The Influence of Alkali and Alkaline Earths on the Working Range for Bioactive Glasses, 1997, https://doi.org/10.1002/(SICI)1097-4636(199707)36:1.
[7] D. Bellucci, E. Veronesi, M. Dominici, V. Cannillo, A new bioactive glass with extremely high crystallization temperature and outstanding biological

performance, Mater. Sci. Eng. C 110 (2020) 110699, https://doi.org/10.1016/J.MSEC.2020.110699.
[8] D. Bellucci, V. Cannillo, A novel bioactive glass containing strontium and magnesium with ultra-high crystallization temperature, Mater. Lett. 213 (2018) 67–70, https://doi.org/10.1016/J.MATLET.2017.11.020.
[9] E. Verné, O. Bretcanu, C. Balagna, C.L. Bianchi, M. Cannas, S. Gatti, C. Vitale-Brovarone, Early stage reactivity and in vitro behavior of silica-based bioactive glasses and glass-ceramics, J. Mater. Sci. Mater. Med. 20 (2009), https://doi.org/10.1007/s10856-008-3537-8.
[10] Á.J. Leite, A.I. Gonçalves, M.T. Rodrigues, M.E. Gomes, J.F. Mano, Strontium-doped bioactive glass nanoparticles in osteogenic commitment, ACS Appl. Mater. Interfaces 10 (2018), https://doi.org/10.1021/acsami.8b06154.
[11] M. Diba, F. Tapia, A.R. Boccaccini, L.A. Strobel, Magnesium-containing bioactive glasses for biomedical applications, Int. J. Appl. Glass Sci. 3 (2012), https://doi.org/10.1111/j.2041-1294.2012.00095.x.
[12] D. Bellucci, A. Sola, R. Salvatori, A. Anesi, L. Chiarini, V. Cannillo, Role of magnesium oxide and strontium oxide as modifiers in silicate-based bioactive glasses: effects on thermal behaviour, mechanical properties and in-vitro bioactivity, Mater. Sci. Eng. C 72 (2017) 566–575, https://doi.org/10.1016/J.MSEC.2016.11.110.
[13] J.F. Stebbins, Structure and dynamics of magnesium in silicate melts: a high-temperature 25Mg nmr study, Am. Mineral. 83 (1998) 1022–1029, https://doi.org/10.2138/AM-1998-9-1010/MACHINEREADABLECITATION/RIS.
[14] K. Shimoda, Y. Tobu, M. Hatakeyama, T. Nemoto, K. Saito, Structural investigation of Mg local environments in silicate glasses by ultra-high field 25Mg 3QMAS NMR spectroscopy, Am. Mineral. 92 (2007) 695–698, https://doi.org/10.2138/AM.2007.2535.
[15] S.J. Watts, R.G. Hill, M.D. O'Donnell, R.V. Law, Influence of magnesia on the structure and properties of bioactive glasses, J. Non-Cryst. Solids 356 (2010), https://doi.org/10.1016/j.jnoncrysol.2009.04.074.
[16] A. Pedone, G. Malavasi, M.C. Menziani, Computational insight into the effect of CaO/MgO substitution on the structural properties of phospho-silicate bioactive glasses, J. Phys. Chem. C 113 (2009) 15723–15730, https://doi.org/10.1021/JP904131T.
[17] P. Jha, K. Singh, Effect of MgO on bioactivity, hardness, structural and optical properties of SiO 2-K 2 O-CaO-MgO glasses, Ceram. Int. 42 (2016) 436–444, https://doi.org/10.1016/j.ceramint.2015.08.128.
[18] M. Magallanes-Perdomo, A.H. De Aza, I. Sobrados, J. Sanz, P. Pena, Structure and properties of bioactive eutectic glasses based on the Ca3(PO4)2–CaSiO3–CaMg(SiO3)2 System, Acta Biomater. 8 (2012) 820–829, https://doi.org/10.1016/J.ACTBIO.2011.10.017.
[19] S.I. Schmitz, B. Widholz, C. Essers, M. Becker, D.U. Tulyaganov, A. Moghaddam, I. Gonzalo de Juan, F. Westhauser, Superior biocompatibility and comparable osteoinductive properties: sodium-reduced fluoride-containing bioactive glass belonging to the CaO–MgO–SiO2 System as a promising alternative to 45S5 bioactive glass, Bioact. Mater. 5 (2020) 55–65, https://doi.org/10.1016/J.BIOACTMAT.2019.12.005.
[20] A. Moghanian, A. Sedghi, A. Ghorbanoghli, E. Salari, The effect of magnesium content on in vitro bioactivity, biological behavior and antibacterial activity of sol–gel derived 58S bioactive glass, Ceram. Int. 44 (2018) 9422–9432, https://doi.org/10.1016/J.CERAMINT.2018.02.159.
[21] N. Kanzaki, K. Onuma, G. Treboux, S. Tsutsumi, A. Ito, Inhibitory effect of magnesium and zinc on crystallization kinetics of hydroxyapatite, J. Phys. Chem. B 104 (2000) 4189–4194, https://doi.org/10.1021/JP9939726.
[22] M.D. O'Donnell, R.G. Hill, Influence of strontium and the importance of glass chemistry and structure when designing bioactive glasses for bone regeneration, Acta Biomater. 6 (2010) 2382–2385, https://doi.org/10.1016/J.ACTBIO.2010.01.006.
[23] J. Isaac, J. Nohra, J. Lao, E. Jallot, Effects of Strontium-Doped Bioactive Glass on the Differentiation of Cultured Osteogenic Cells, 2014, https://doi.org/10.22203/eCM.v021a11.
[24] M.D. O'Donnell, P.L. Candarlioglu, C.A. Miller, E. Gentleman, M.M. Stevens, Materials characterisation and cytotoxic assessment of strontium-substituted bioactive glasses for bone regeneration, J. Mater. Chem. 20 (2010) 8934–8941, https://doi.org/10.1039/C0JM01139H.
[25] S. Kargozar, M. Montazerian, E. Fiume, F. Baino, Multiple and promising applications of strontium (Sr)-Containing bioactive glasses in bone tissue engineering, Front. Bioeng. Biotechnol. 7 (2019) 453733, https://doi.org/10.3389/FBIOE.2019.00161.
[26] K. Fujikura, N. Karpukhina, T. Kasuga, D.S. Brauer, R.G. Hill, R.V. Law, Influence of strontium substitution on structure and crystallisation of Bioglass® 45S5, J. Mater. Chem. 22 (2012) 7395–7402, https://doi.org/10.1039/C2JM14674F.
[27] J.M. Tainio, D.A.A. Salazar, A. Nommeots-Nomm, C. Roiland, B. Bureau, D. R. Neuville, D.S. Brauer, J. Massera, Structure and in vitro dissolution of Mg and Sr containing borosilicate bioactive glasses for bone tissue engineering, J. Non-Cryst. Solids 533 (2020) 119893, https://doi.org/10.1016/J.JNONCRYSOL.2020.119893.
[28] W.C. Oliver, G.M. Pharr, An improved technique for determining hardness and elastic modulus using load and displacement sensing indentation experiments, J. Mater. Res. 7 (1992), https://doi.org/10.1557/jmr.1992.1564.
[29] C. Ohtsuki, H. Kushitani, T. Kokubo, S. Kotani, T. Yamamuro, Apatite Formation on the surface of ceravital-type glass-ceramic in the body, J. Biomed. Mater. Res. 25 (1991) 1363–1370, https://doi.org/10.1002/JBM.820251105.
[30] T. Kokubo, H. Kushitani, S. Sakka, T. Kitsugi, T. Yamamuro, Solutions able to reproduce in vivo surface-structure changes in bioactive glass-ceramic A-W3, J. Biomed. Mater. Res. 24 (1990) 721–734, https://doi.org/10.1002/JBM.820240607.
[31] T. Kokubo, H. Takadama, How useful is SBF in predicting in vivo bone bioactivity? Biomaterials 27 (2006) https://doi.org/10.1016/j.biomaterials.2006.01.017.
[32] International Standard Organization ISO 10993-12:2021 - Biological Evaluation of Medical Devices — Part 12: Sample Preparation and Reference Materials.
[33] F. Boraldi, A. Bartolomeo, C. Di Bari, A. Cocconi, D. Quaglino, Donor's age and replicative senescence favour the in-vitro mineralization potential of human fibroblasts, Exp. Gerontol. 72 (2015) 218–226, https://doi.org/10.1016/J.EXGER.2015.10.009.
[34] M. Feoktistova, P. Geserick, M. Leverkus, Crystal violet assay for determining viability of cultured cells, Cold Spring Harb. Protoc. 2016 (2016) 343–346, https://doi.org/10.1101/PDB.PROT087379.
[35] O. Bretcanu, X. Chatzistavrou, K. Paraskevopoulos, R. Conradt, I. Thompson, A. R. Boccaccini, Sintering and crystallisation of 45S5 Bioglass® powder, J. Eur. Ceram. Soc. 29 (2009), https://doi.org/10.1016/j.jeurceramsoc.2009.06.035.
[36] A.R. Boccaccini, Q. Chen, L. Lefebvre, L. Gremillard, J. Chevalier, Sintering, crystallisation and biodegradation behaviour of bioglass®-derived glass-ceramics, Faraday Discuss 136 (2007), https://doi.org/10.1039/b616539g.
[37] J. Massera, S. Fagerlund, L. Hupa, M. Hupa, Crystallization mechanism of the bioactive glasses, 45S5 and S53P4, J. Am. Ceram. Soc. 95 (2012), https://doi.org/10.1111/j.1551-2916.2011.05012.x.
[38] G. Strömberg, L. Aalto-Setälä, P. Uppstu, R. Björkenheim, J. Pajarinen, E. Eriksson, N.C. Lindfors, L. Hupa, Development and characterization of non-coated and PLGA-coated S53P4 and S59 bioactive glass scaffolds for treatment of load-bearing defects, Biomedical Materials & Devices (2023), https://doi.org/10.1007/s44174-023-00099-4.
[39] H. Arstila, E. Vedel, L. Hupa, M. Hupa, Factors affecting crystallization of bioactive glasses, J. Eur. Ceram. Soc. 27 (2007), https://doi.org/10.1016/j.jeurceramsoc.2006.04.017.
[40] M. Fabert, N. Ojha, E. Erasmus, M. Hannula, M. Hokka, J. Hyttinen, J. Rocherullé, I. Sigalas, J. Massera, Crystallization and sintering of borosilicate bioactive glasses for application in tissue engineering, J. Mater. Chem. B 5 (2017), https://doi.org/10.1039/c7tb00106a.
[41] J. Massera, S. Fagerlund, L. Hupa, M. Hupa, Crystallization mechanism of the bioactive glasses, 45S5 and S53P4, J. Am. Ceram. Soc. 95 (2012), https://doi.org/10.1111/j.1551-2916.2011.05012.x.
[42] L. Lefebvre, L. Gremillard, J. Chevalier, R. Zenati, D. Bernache-Assolant, Sintering behaviour of 45S5 bioactive glass, Acta Biomater. 4 (2008), https://doi.org/10.1016/j.actbio.2008.05.019.
[43] Q.Z. Chen, I.D. Thompson, A.R. Boccaccini, 45S5 bioglass®-derived glass-ceramic scaffolds for bone tissue engineering, Biomaterials 27 (2006), https://doi.org/10.1016/j.biomaterials.2005.11.025.
[44] R. Björkenheim, E. Jämsen, E. Eriksson, P. Uppstu, L. Aalto-Setälä, L. Hupa, K. K. Eklund, M. Ainola, N.C. Lindfors, J. Pajarinen, Sintered S53p4 bioactive glass scaffolds have anti-inflammatory properties and stimulate osteogenesis in vitro, Eur. Cell. Mater. 41 (2021), https://doi.org/10.22203/eCM.v041a02.
[45] H. Arstila, L. Hupa, K.H. Karlsson, M. Hupa, Influence of heat treatment on crystallization of bioactive glasses, J. Non-Cryst. Solids 354 (2008), https://doi.org/10.1016/j.jnoncrysol.2007.06.092.
[46] N. Lotfibakhshaiesh, D.S. Brauer, R.G. Hill, Bioactive glass engineered coatings for Ti6Al4V alloys: influence of strontium substitution for calcium on sintering behaviour, in: Proceedings of the Journal of Non-Crystalline Solids, 356, 2010.
[47] C. Volzone, F.M. Stábile, Structural changes by thermal treatment up to glass obtention of P2O5-Na2O-CaO-SiO2 compounds with Bioglass composition types, New J. Glass Ceram. 3 (2013).
[48] C. Berbecaru, H.V. Alexandru, G.E. Stan, D.A. Marcov, I. Pasuk, A. Ianculescu, First stages of bioactivity of glass-ceramics thin films prepared by magnetron sputtering technique, Mater. Sci. Eng., B 169 (2010), https://doi.org/10.1016/j.mseb.2010.01.007.
[49] D.C. Clupper, L.L. Hench, Crystallization kinetics of tape cast bioactive glass 45S5, J. Non-Cryst. Solids 318 (2003), https://doi.org/10.1016/S0022-3093(02)01857-4.
[50] A.R. Boccaccini, Q. Chen, L. Lefebvre, L. Gremillard, J. Chevalier, Sintering, crystallisation and biodegradation behaviour of bioglass®-derived glass-ceramics, Faraday Discuss 136 (2007), https://doi.org/10.1039/b616539g.
[51] M. Montazerian, A. Shearer, J.C. Mauro, Perspectives on the impact of crystallization in bioactive glasses and glass-ceramics, International Journal of Ceramic Engineering and Science (2023), https://doi.org/10.1002/ces2.10194.
[52] S.R. Gavinho, A.S. Pádua, L.I.V. Holz, I. Sá-Nogueira, J.C. Silva, J.P. Borges, M. A. Valente, M.P.F. Graça, Bioactive glasses containing strontium or magnesium ions to enhance the biological response in bone regeneration, Nanomaterials 13 (2023), https://doi.org/10.3390/nano13192717.
[53] A. Stiller, M. Engblom, E. Vainio, L. Hupa, Understanding the crystallization behavior of bioactive glass S53P4 powder compacts under various heating conditions, J. Non-Cryst. Solids 644 (2024), https://doi.org/10.1016/j.jnoncrysol.2024.123178.
[54] C. Yang, J. Bai, G. Wang, H. Wang, S. Ma, Effect of Na2O content on wettability, crystallization and performances of sealing glass, J. Mater. Res. Technol. 23 (2023) 4117–4134, https://doi.org/10.1016/J.JMRT.2023.02.073.
[55] L.L. Hench, Bioceramics, J. Am. Ceram. Soc. 81 (1998) 1705–1728.
[56] G. El Damrawi, R.M. Ramadan, M. El Baiomy, Effect of SrO on the structure of apatite and wollastonite phases of Na2O-CaO-SiO2-P2O5 glass System, New J. Glass Ceram. 11 (2021) 45–56, https://doi.org/10.4236/njgc.2021.112003.

[57] F. Sharifianjazi, M. Moradi, A. Abouchenari, A.H. Pakseresht, A. Esmaeilkhanian, M. Shokouhimehr, M. Shahedi Asl, Effects of Sr and Mg dopants on biological and mechanical properties of SiO2–CaO–P2O5 bioactive glass, Ceram. Int. 46 (2020), https://doi.org/10.1016/j.ceramint.2020.06.030.
[58] I. Cacciotti, Bivalent cationic ions doped bioactive glasses: the influence of magnesium, zinc, strontium and copper on the physical and biological properties, J. Mater. Sci. 52 (2017), https://doi.org/10.1007/s10853-017-1010-0.
[59] Y.C. Fredholm, N. Karpukhina, R.V. Law, R.G. Hill, Strontium containing bioactive glasses: glass structure and physical properties, in: Proceedings of the Journal of Non-Crystalline Solids, 356, 2010.
[60] V. Cannillo, L. Esposito, E. Rambaldi, A. Sola, A. Tucci, Effect of porosity on the elastic properties of porcelainized stoneware tiles by a multi-layered model, Ceram. Int. 35 (2009), https://doi.org/10.1016/j.ceramint.2007.10.015.
[61] V. Cannillo, M. Montorsi, C. Siligardi, A. Sola, G. de Portu, L. Micele, G. Pezzotti, Microscale computational simulation and experimental measurement of thermal residual stresses in glass–alumina functionally graded materials, J. Eur. Ceram. Soc. 26 (2006) 1411–1419, https://doi.org/10.1016/J.JEURCERAMSOC.2005.02.012.
[62] V. Cannillo, C. Leonelli, A.R. Boccaccini, Numerical models for thermal residual stresses in Al2O3 platelets/borosilicate glass matrix composites, Mater. Sci. Eng., A 323 (2002) 246–250, https://doi.org/10.1016/S0921-5093(01)01345-4.
[63] F.G. Mecca, D. Bellucci, V. Cannillo, Effect of thermal treatments and ion substitution on sintering and crystallization of bioactive glasses: a review, Materials 16 (2023) 4651, https://doi.org/10.3390/MA16134651. Page 4651 2023, 16.
[64] M. Zarur, A. Seijo-Rabina, A. Goyanes, A. Concheiro, C. Alvarez-Lorenzo, PH-responsive scaffolds for tissue regeneration: in vivo performance, Acta Biomater. 168 (2023).
[65] W.K. Ramp, L.G. Lenz, K.K. Kaysinger, Medium PH modulates matrix, mineral, and energy metabolism in cultured chick bones and osteoblast-like cells, Bone Miner. 24 (1994) 59–73, https://doi.org/10.1016/S0169-6009(08)80131-6.
[66] I. Allan, H. Newman, M. Wilson, Antibacterial activity of particulate Bioglass® against supra- and subgingival bacteria, Biomaterials 22 (2001) 1683–1687, https://doi.org/10.1016/S0142-9612(00)00330-6.
[67] D. Zhang, O. Leppäranta, E. Munukka, H. Ylänen, M.K. Viljanen, E. Eerola, M. Hupa, L. Hupa, Antibacterial effects and dissolution behavior of six bioactive glasses, J. Biomed. Mater. Res. 93 (2010) 475–483, https://doi.org/10.1002/JBM.A.32564.
[68] A. El-Ghannam, P. Ducheyne, I.M. Shapiro, Formation of surface reaction products on bioactive glass and their effects on the expression of the osteoblastic phenotype and the deposition of mineralized extracellular matrix, Biomaterials 18 (1997) 295–303, https://doi.org/10.1016/S0142-9612(96)00059-2.
[69] S.M. Rabiee, N. Nazparvar, M. Azizian, D. Vashaee, L. Tayebi, Effect of ion substitution on properties of bioactive glasses: a review, Ceram. Int. 41 (2015).
[70] A. Brandao-Burch, J.C. Utting, I.R. Orriss, T.R. Arnett, Acidosis inhibits bone formation by osteoblasts in vitro by preventing mineralization, Calcif. Tissue Int. 77 (2005) 167–174, https://doi.org/10.1007/S00223-004-0285-8.
[71] A. Antonakos, E. Liarokapis, T. Leventouri, Micro-Raman and FTIR studies of synthetic and natural apatites, Biomaterials 28 (2007) 3043–3054, https://doi.org/10.1016/J.BIOMATERIALS.2007.02.028.
[72] G. Penel, G. Leroy, C. Rey, E. Bres, MicroRaman spectral study of the PO4 and CO3 vibrational modes in synthetic and biological apatites, Calcif. Tissue Int. 63 (1998) 475–481, https://doi.org/10.1007/S002239900561.
[73] A. Awonusi, M.D. Morris, M.M.J. Tecklenburg, Carbonate assignment and calibration in the Raman spectrum of apatite, Calcif. Tissue Int. 81 (2007) 46–52, https://doi.org/10.1007/S00223-007-9034-0/FIGURES/5.
[74] E.C. Ziemath, M.A. Aegerter, Raman and infrared investigations of glass and glass-ceramics with composition 2Na2O. 1CaO. 3SiO2, J. Mater. Res. 9 (1994) 216–225, https://doi.org/10.1557/JMR.1994.0216.
[75] D. Bellucci, A. Sola, V. Cannillo, Low temperature sintering of innovative bioactive glasses, J. Am. Ceram. Soc. 95 (2012) 1313–1319, https://doi.org/10.1111/J.1551-2916.2012.05100.X.
[76] L.L. Hench, Bioceramics: from concept to clinic, J. Am. Ceram. Soc. 74 (1991) 1487–1510, https://doi.org/10.1111/J.1151-2916.1991.TB07132.X.
[77] H. Liu, H. Yazici, C. Ergun, T.J. Webster, H. Bermek, An in vitro evaluation of the Ca/P ratio for the cytocompatibility of nano-to-micron particulate calcium phosphates for bone regeneration, Acta Biomater. 4 (2008) 1472–1479, https://doi.org/10.1016/J.ACTBIO.2008.02.025.
[78] S. Padilla, J. Román, S. Sánchez-Salcedo, M. Vallet-Regí, Hydroxyapatite/SiO2-CaO-P2O5 glass materials: in vitro bioactivity and biocompatibility, Acta Biomater. 2 (2006) 331–342, https://doi.org/10.1016/J.ACTBIO.2006.01.006.
[79] X. Liu, D.P. Rodeheaver, J.C. White, A.M. Wright, L.M. Walker, F. Zhang, S. Shannon, A comparison of in vitro cytotoxicity assays in medical device regulatory studies, Regul. Toxicol. Pharmacol. 97 (2018) 24–32, https://doi.org/10.1016/J.YRTPH.2018.06.003.
[80] G. Ciapetti, E. Cenni, L. Pratelli, A. Pizzoferrato, In vitro evaluation of cell/biomaterial interaction by MTT assay, Biomaterials 14 (1993) 359–364, https://doi.org/10.1016/0142-9612(93)90055-7.
[81] Arcos Navarrete, D.; Vallet-Regí, M. Bioactive Glasses : Properties, Composition and Recent Applications.
[82] A.J. Salinas, M. Vallet-Regi, J. Heikkilä, Use of bioactive glasses as bone substitutes in orthopedics and traumatology, Bioactive Glasses: Materials, Properties and Applications (2018) 337–364, https://doi.org/10.1016/B978-0-08-100936-9.00014-9. Second Edition.
[83] Y. Liu, X. Liu, H. Guo, X. Wang, A. Li, D. Qiu, Q. Gu, 3D bioprinting Bioglass to construct vascularized full-thickness skin substitutes for wound healing, Mater Today Bio 24 (2023), https://doi.org/10.1016/J.MTBIO.2023.100899.
[84] C. Viennet, P. Muret, Fibroblast evaluation: extracellular matrix synthesis, Measuring the Skin (2015) 1–5, https://doi.org/10.1007/978-3-319-26594-0_124-1.
[85] F. Boraldi, F.D. Lofaro, S. Bonacorsi, A. Mazzilli, M. Garcia-Fernandez, D. Quaglino, The role of fibroblasts in skin homeostasis and repair, Biomedicines 12 (2024) 1586, https://doi.org/10.3390/BIOMEDICINES12071586. Page 1586 2024, 12.
[86] A. Anesi, M. Ferretti, R. Salvatori, D. Bellucci, F. Cavani, M. Di Bartolomeo, C. Palumbo, V. Cannillo, In-vivo evaluations of bone regenerative potential of two novel bioactive glasses, J. Biomed. Mater. Res. 111 (2023) 1264–1278, https://doi.org/10.1002/JBM.A.37526.
[87] D. Bellucci, E. Veronesi, M. Dominici, V. Cannillo, On the in vitro biocompatibility testing of bioactive glasses, Materials 13 (2020) 1816, https://doi.org/10.3390/MA13081816. Page 1816 2020, 13.
[88] C. Rodrigues, L.I.S. Naasani, C. Zanatelli, T.C. Paim, J.G. Azevedo, J.C. de Lima, M. da Cruz Fernandes, S. Buchner, M.R. Wink, Bioglass 45S5: structural characterization of short range order and analysis of biocompatibility with adipose-derived mesenchymal stromal cells in vitro and in vivo, Mater. Sci. Eng. C 103 (2019) 109781, https://doi.org/10.1016/J.MSEC.2019.109781.
[89] A.S. Bakry, H. Takahashi, M. Otsuki, J. Tagami, Evaluation of new treatment for incipient enamel demineralization using 45S5 Bioglass, Dent. Mater. 30 (2014) 314–320, https://doi.org/10.1016/J.DENTAL.2013.12.002.
[90] A.S. Bakry, Y. Tamura, M. Otsuki, S. Kasugai, K. Ohya, J. Tagami, Cytotoxicity of 45S5 Bioglass paste used for dentine hypersensitivity treatment, J. Dent. 39 (2011) 599–603, https://doi.org/10.1016/J.JDENT.2011.06.003.
[91] M. Handel, T.R. Hammer, P. Nooeaid, A.R. Boccaccini, D. Hoefer, 45S5-Bioglass®-Based 3D-Scaffolds Seeded with Human Adipose Tissue-Derived Stem Cells Induce in Vivo Vascularization in the CAM Angiogenesis Assay, vol. 19, 2013, pp. 2703–2712, https://doi.org/10.1089/TEN.TEA.2012.0707. https://home.liebertpub.com/tea.
[92] H. Yu, J. Peng, Y. Xu, J. Chang, H. Li, Bioglass activated skin tissue engineering constructs for wound healing, ACS Appl. Mater. Interfaces 8 (2016) 703–715, https://doi.org/10.1021/ACSAMI.5B09853/ASSET/IMAGES/LARGE/AM-2015-09853K_0012.JPEG.
[93] S. Naseri, W.C. Lepry, S.N. Nazhat, Bioactive glasses in wound healing: hope or hype? J. Mater. Chem. B 5 (2017) 6167–6174, https://doi.org/10.1039/C7TB01221G.
[94] I.A. Silver, J. Deas, M. Erecińska, Interactions of bioactive glasses with osteoblasts in vitro: effects of 45S5 Bioglass®, and 58S and 77S bioactive glasses on metabolism, intracellular ion concentrations and cell viability, Biomaterials 22 (2001) 175–185, https://doi.org/10.1016/S0142-9612(00)00173-3.
[95] R.M. Day, A.R. Boccaccini, S. Shurey, J.A. Roether, A. Forbes, L.L. Hench, S. M. Gabe, Assessment of polyglycolic acid mesh and bioactive glass for soft-tissue engineering scaffolds, Biomaterials 25 (2004) 5857–5866, https://doi.org/10.1016/j.biomaterials.2004.01.043.
[96] R. Detsch, S. Alles, J. Hum, P. Westenberger, F. Sieker, D. Heusinger, C. Kasper, A. R. Boccaccini, Osteogenic differentiation of umbilical cord and adipose derived stem cells onto highly porous 45S5 bioglass®-based scaffolds, J. Biomed. Mater. Res. 103 (2015) 1029–1037, https://doi.org/10.1002/JBM.A.35238.
[97] M. Cerruti, D. Greenspan, K. Powers, Effect of PH and ionic strength on the reactivity of Bioglass® 45S5, Biomaterials 26 (2005) 1665–1674, https://doi.org/10.1016/J.BIOMATERIALS.2004.07.009.
[98] M. Rabe, D. Verdes, S. Seeger, Understanding protein adsorption phenomena at solid surfaces, Adv. Colloid Interface Sci. 162 (2011) 87–106, https://doi.org/10.1016/J.CIS.2010.12.007.
[99] I.D. Xynos, M.V.J. Hukkanen, J.J. Batten, L.D. Buttery, L.L. Hench, J.M. Polak, Bioglass ®45S5 stimulates osteoblast turnover and enhances bone formation in vitro: implications and applications for bone tissue engineering, Calcif. Tissue Int. 67 (2000) 321–329, https://doi.org/10.1007/S002230001134/METRICS.
[100] L. de Araujo Bastos Santana, P.H. Oliveira Junior, C. Damia, D. dos Santos Tavares, E.A. dos Santos, Bioactivity in SBF versus trace element effects: the isolated role of Mg2+ and Zn2+ in osteoblast behavior, Mater. Sci. Eng., C 118 (2021), https://doi.org/10.1016/J.MSEC.2020.111320.
[101] H. Zreiqat, C.R. Howlett, A. Zannettino, P. Evans, G. Schulze-Tanzil, C. Knabe, M. Shakibaei, Mechanisms of magnesium-stimulated adhesion of osteoblastic cells to commonly used orthopaedic implants, J. Biomed. Mater. Res. 62 (2002) 175–184, https://doi.org/10.1002/JBM.10270.
[102] D.D. Schlaepfer, S.K. Hanks, T. Hunter, P. Geer, Van der integrin-mediated signal transduction linked to ras pathway by GRB2 binding to focal adhesion kinase, Nature 372 (1994) 786–791, https://doi.org/10.1038/372786a0, 6508 1994, 372.
[103] R. Amberg, A. Elad, D. Rothamel, T. Fienitz, G. Szakacs, S. Heilmann, F. Witte, Design of a migration assay for human gingival fibroblasts on biodegradable magnesium surfaces, Acta Biomater. 79 (2018) 158–167, https://doi.org/10.1016/J.ACTBIO.2018.08.034.
[104] P.A. Dash, S. Mohanty, S.K. Nayak, A review on bioactive glass, its modifications and applications in healthcare sectors, J. Non-Cryst. Solids 614 (2023) 122404, https://doi.org/10.1016/J.JNONCRYSOL.2023.122404.
[105] L. Lefebvre, J. Chevalier, L. Gremillard, R. Zenati, G. Thollet, D. Bernache-Assolant, A. Govin, Structural transformations of bioactive glass 45S5 with thermal treatments, Acta Mater. 55 (2007) 3305–3313, https://doi.org/10.1016/J.ACTAMAT.2007.01.029.

[106] J. McAndrew, C. Efrimescu, E. Sheehan, D. Niall, Through the looking glass; bioactive glass S53P4 (BonAlive®) in the treatment of chronic osteomyelitis, Ir. J. Med. Sci. 182 (2013) 509–511, https://doi.org/10.1007/S11845-012-0895-5/FIGURES/1.

[107] N.C. Lindfors, Clinical experience on bioactive glass S53P4 in reconstructive surgery in the upper extremity showing bone remodelling, vascularization, cartilage repair and antibacterial properties of S53P4, J. Biotechnol. Biomater. 1 (2011), https://doi.org/10.4172/2155-952X.1000111.

[108] G.J. Todaro, H. Green, Quantitative studies of the growth of mouse embryo cells in culture and their development into established lines, JCB (J. Cell Biol.) 17 (1963) 299–313, https://doi.org/10.1083/JCB.17.2.299.

[109] R. Pérez-Tanoira, T.J. Kinnari, T. Hyyrynen, A. Soininen, L. Pietola, V.M. Tiainen, Y.T. Konttinen, A.A. Aarnisalo, Effects of S53P4 bioactive glass on osteoblastic cell and biomaterial surface interaction, J. Mater. Sci. Mater. Med. 26 (2015) 1–11, https://doi.org/10.1007/S10856-015-5568-2/TABLES/2.

[110] N.A.P. van Gestel, F. Gabriels, J.A.P. Geurts, D.J.W. Hulsen, C.E. Wyers, J.P. van de Bergh, K. Ito, S. Hofmann, J.J. Arts, B. van Rietbergen, The implantation of bioactive glass granules can contribute the load-bearing capacity of bones weakened by large cortical defects, Materials 12 (2019) 3481, https://doi.org/10.3390/MA12213481. Page 3481 **2019**, 12.